



### FRAS 1.1.3; Weld Residual Stresses

## Practical inclusion and behaviour of welding residual stresses in structural integrity analyses of NPP primary circuit components

Author(s): Otso Cronvall

Confidentiality: Public

|   |   |
|---|---|
| <b>Report's title</b><br>Practical inclusion and behaviour of welding residual stresses in structural integrity analyses of NPP primary circuit components  |   |
| <b>Customer, contact person, address</b><br>State Nuclear Waste Management Fund (VYR), Swedish Nuclear Power Inspectorate (SKI) and VTT   | <b>Order reference</b>                              |
| <b>Project name</b><br>FRAS 1.1.3; Weld Residual Stresses   | <b>Project number/Short name</b><br>32418/FRAS 09   |
| <b>Author(s)</b><br>Otso Cronvall   | <b>Pages</b><br>53 / 0                              |
| <b>Keywords</b><br>WRSs, NPP, reactor circuit component welds, FEM, fracture mechanics, SINTAP, IGSCC, CGR  | <b>Report identification code</b><br>VTT-R-00962-09 |
| <b>Summary</b><br><p>This study concerns the welding process induced residual stresses in Nuclear Power Plant (NPP) reactor circuit component welds, and their practical inclusion in structural integrity analyses. The goal of the work here is to study via numerical simulations how the welding residual stresses (WRSs) alter over the years in plant operation in primary circuit component welds (e.g. to see if and how much they decrease), due to various typical/anticipated transient load cases. When having such stress results, it is then examined what is their impact to the corresponding simulated crack growth rates (CGRs). In the latter analyses a fracture mechanics based analysis tool VTTBESIT, which is partly developed at VTT, is used.</p> <p>When looking for a suitable applicable WRS procedure to use in the numerical WRS simulations, the following fitness-for-service procedures were considered: the ASME recommendations [2, 3], the British Standard BS 7910: 1999 [4], the R6 Method, Revision 4 [5], the SAQ handbook [6], the SINTAP Procedure [7, 8], the API 579 procedure [9] and the FITNET Procedure [10]. The selected WRS type here for numerical simulations is as-welded state. The WRS definitions included in the mentioned procedures are based both on the available experimental data and FEM analysis results. The published experimental WRS data have a substantial scatter. Consequently the defined WRS distributions have been conservatively developed as tensile upper bound solutions based on the data.</p> <p>One unfortunate departure from realism in case of some of the more recent WRS procedures, e.g. R6 Method Rev. 4 and FITNET, is that in the transverse to weld direction the WRSs are mostly not self-balancing. While making local crack growth calculations with a fracture mechanics based analysis tool this feature may not pose remarkable problems, but in case of corresponding 2D or 3D FEM analyses it is quite the other way around, as in order to achieve equilibrium FEM automatically modifies the WRSs towards self-balanced distributions over the component model walls, and thus the original WRS distributions are not maintained.</p> <p>In the light of the WRS analysis results presented in ref. [13], by the author of this report, only ASME recommendations [2, 3] and SINTAP procedure [7, 8] in all cases, and SAQ handbook in most cases [6], give as-welded state WRS distributions that are self-balancing in the transverse to weld direction. Of them the least over conservative WRS procedure appears to be SINTAP, which was also selected to be used for defining the as-welded state WRSs to be used in the FEM simulations in this study.</p> <p>The type of the selected component assembly to the FEM analyses is a safe-end joined with welds to a nozzle and pipe, resembling those that connect the feed water system to the Reactor Pressure Vessel (RPV) in Boiling Water Reactor (BWR) units. The wall thickness of the safe-end/pipe weld examined in more detail is 16 mm.</p> <p>A history of anticipated load transients was analysed with advanced FEM code Abaqus, version 6.8-2 [11, 12], with an axisymmetric model. The load transients were included in a single analysis run in a realistic chronological order and separated by static loading conditions long enough for steady state to take place. Thus the effect of structural memory, i.e. the effect to each present elastic-plastic stress/strain state of all earlier loads, was fully included. All in all there were 28 analysed load transients of which 16 load events were assembled, most of them being full load cycles. The only considered static load case is operational conditions. Of the load types provided by Abaqus, the Body Force was selected for simulating WRSs in the safe-end/pipe joint weld region of the FEM analysis model. The examination was limited to concern only transverse to weld WRSs, as worldwide more than 90 % of the encountered/detected primary circuit piping crack cases have been oriented longitudinally to weld, see e.g. ref. [22], and it is mainly transverse stresses that make such cracks grow.</p> |   |

According to FEM results, after the analysed load events the transverse to weld WRSs in the weld centre line have decreased in and near the inner and outer surface approximately 50 MPa. Within the wall the WRSs levels on the other hand climbed to some extent higher, somewhat suggesting that the continuing distribution of the maximum WRSs to the adjacent material regions occurs also in the through weld wall thickness direction. The relaxing of the WRSs was on the weld edges approximately of the same scale as on the centre line.

For the examined safe-end/pipe joint weld two crack growth analysis cases were considered:

1. The WRS component of the stresses acting in the weld remaining at as-welded state as defined according to the SINTAP procedure [7, 8], and with other stresses as caused by process loads. In this case all stress components are set to remain as such, i.e. they are time independent. Here the WRSs were added to other stress components by superposition to obtain the total stress distribution.
2. The WRS component and other stresses are taken time dependently from the results of the performed FEM analyses. In this case it was assumed that the stress distributions within the weld region remain as they are after the last analysed load event.


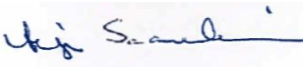

In both crack growth analyses, performed with VTTBESIT, the considered crack postulate is a circumferentially oriented inner semi-elliptic surface crack, with aspect ratio of 1/3. The dimensions of the initial crack postulate are: depth x length = 0.1 x 0.6 mm. The analyses cover an assumed operational plant lifetime of 60 years. In the crack growth analyses the considered degradation mechanism and load case were IGSCC and static operational conditions, respectively.

The calculated crack growth was for both analysis cases relatively quick, once the crack depth had exceeded approximately 1.5 mm. As for analysis case 2, the calculated CGR was to some extent slower than for analysis case 1, where the as-welded state WRSs and other stress components were kept in their original values throughout the analysis. For instance, in case 2 the crack grows to 50 % and 90 % depths of wall thickness in 8.2 and 10.6 years, whereas the same results for case 1 are 7.7 and 9.9 years, respectively. The slowing down of the CGR in both analysed cases when approaching the outer wall surface is caused by the compressive WRS values in that part of the wall, the compression reaching the maximum value in the outer surface.

The next step in the numerical WRS simulations could be to use a suitably optimised 3D FEM model in the analyses, or a coarser global 3D model in combination with a local but large enough and more densely meshed sub-model containing the region of interest, i.e. a weld. Also, to simulate the local WRS distributions, it could be tried to use such values for the coefficient of thermal expansion in the weld region of the FEM model that the resulting stress field within the covered temperature range would match the desired WRS distribution. One way to further examine how the relatively high as-welded state WRSs alter over the years in plant operation in primary circuit component welds would be to carry out a literature study on the subject. This will be realised in the next phase of this project.

Also, the examined load history consisting of various anticipated load transients could be extended so as to cover more simulated years of simulated plant operation, and on the other hand a larger variety of different load transients, than in this study. A primary circuit component weld of other type than considered here could be examined next as well, e.g. a nozzle/safe-end joint weld.

|                 |        |
|-----------------|--------|
| Confidentiality | Public |
|-----------------|--------|

|   |   |   |
|---|---|---|
| Espoo 2.6.2009  |   |   |
| Signatures  | Signatures  | Signatures  |
|  |  |  |
| Written by Otso Cronvall<br>Research Scientist                                      | Reviewed by Arja Saarenheimo<br>Senior Research Scientist                           | Accepted by Eila Lehmus<br>Technology Manager   |

|   |
|---|
| VTT's contact address<br>P.O. Box 1000, 02044 VTT |
|---|

|  |
|--|
| Distribution (customer and VTT)<br>SAFIR2010 Reference Group 6 (Structural Safety of Reactor Circuit);<br>SAFIR2010 FRAS Ad-Hoc Group;<br>VTT: Archive (2) |
|--|

|   |
|---|
| <i>The use of the name of the VTT Technical Research Centre of Finland (VTT) in advertising or publication in part of this report is only permissible with written authorisation from the VTT Technical Research Centre of Finland.</i> |
|---|

## Foreword

This report has been prepared under the research project FRAS 1.1.3; Weld Residual Stresses, which concerns welding process induced residual stress distributions in Nuclear Power Plant (NPP) reactor circuit component welds. The project is a part of SAFIR2010, which is a national nuclear energy research program. FRAS 1.1.3 project work in 2008 was funded by the State Nuclear Waste Management Fund (VYR), the Swedish Nuclear Power Inspectorate (SKI), which as of 1.7.2008 has become a part of the Swedish Radiation Safety Authority (Strålsäkerhetsmyndigheten, SSM), and the Technical Research Centre of Finland (VTT). The work was carried out at VTT. The author of the report expresses his gratitude to Mr Paul Smeekes from Teollisuuden Voima Oy (TVO) for valuable co-operation.

Espoo 2.6.2009

Author

# Contents

|  |    |
|--|----|
| Foreword .....   | 3  |
| List of symbols and abbreviations.....   | 5  |
| 1 Introduction and goal .....  | 7  |
| 2 Brief introduction to WRSs and their relieving .....                                       | 9  |
| 2.1 Introduction to WRSs .....   | 9  |
| 2.2 On the conditions/treatments that relieve WRSs in NPP components .....                   | 10 |
| 3 On the selection of suitable WRS assessment procedure for numerical simulations.....       | 12 |
| 3.1 Applicability of commonly used WRS assessment procedures for numerical simulations ..... | 12 |
| 3.2 WRSs according to SINTAP procedure .....   | 13 |
| 4 Numerical simulations of WRSs in a BWR primary circuit component .....                     | 22 |
| 4.1 Analysis input data.....   | 22 |
| 4.1.1 Geometry .....   | 22 |
| 4.1.2 Material properties .....  | 23 |
| 4.1.3 Loads .....  | 25 |
| 4.2 Heat transfer and stress/strain analyses.....  | 29 |
| 4.2.1 FEM model and boundary conditions.....   | 30 |
| 4.2.2 Aspects concerning modelling of WRSs with FEM .....                                    | 32 |
| 4.2.3 Summary of FEM analysis results.....   | 35 |
| 5 Fracture mechanics based crack growth analyses including WRS distributions...40            |    |
| 5.1 Crack growth analysis input data, analysis procedure and analysis tool.....              | 40 |
| 5.2 Crack growth analysis results .....  | 42 |
| 6 Summary, conclusions and suggestions for further research .....                            | 45 |
| References .....   | 51 |

## List of symbols and abbreviations

### Latin symbols

|            |   |
|------------|---|
| $a$        | Crack depth   |
| $c$        | Half of crack length  |
| $c$        | Specific heat   |
| $C$        | Parameter in the stress corrosion cracking rate equation                                  |
| $E$        | Young's modulus   |
| $K_I$      | Mode I stress intensity factor (SIF-I)  |
| $n$        | Exponent in the stress corrosion cracking rate equation                                   |
| $q$        | Weld arc power acc. to SINTAP   |
| $R$        | Outer pipe radius acc. to SINTAP  |
| $S_m$      | Design stress acc. to ASME code   |
| $S_u$      | Tensile strength acc. to ASME code  |
| $S_y$      | Yield strength acc. to ASME code  |
| $r_0$      | Radius of the yield zone  |
| $t$        | Time  |
| $t$        | Pipe wall thickness acc. to SINTAP  |
| $t_{wall}$ | Component wall thickness  |
| $T$        | Temperature   |
| $v$        | Weld travel speed acc. to SINTAP  |
| $z$        | Radial coordinate through wall having origin at the outer pipe surface acc. to SINTAP     |
| $z_o$      | Through thickness depth of the tensile residual stress zone in repair weld acc. to SINTAP |
| $z_r$      | Repair weld depth acc. to SINTAP  |

### Greek symbols

|                  |  |
|------------------|--|
| $\alpha_T$       | Coefficient of thermal expansion                                       |
| $\alpha_{HT}$    | Heat transfer coefficient  |
| $\phi$           | Outer diameter   |
| $\lambda$        | Thermal conductivity   |
| $\nu$            | Poisson's coefficient  |
| $\rho$           | Material density   |
| $\sigma_R^{L,B}$ | Longitudinal weld residual stress at the pipe wall bore acc. to SINTAP |
| $\sigma_R^{L,O}$ | Longitudinal residual stress at the outer surface acc. to SINTAP       |
| $\sigma_R^T$     | Axial weld residual stress acc. to SINTAP                              |
| $\sigma_R^{T,O}$ | Axial weld residual stress at outer surface acc. to SINTAP             |
| $\sigma_y$       | Yield stress   |
| $\sigma_{yp}$    | Parent metal typical yield stress acc. to SINTAP                       |
| $\sigma_{yw}$    | Weld metal typical yield stress acc. to SINTAP                         |
| $\sigma_y^*$     | Lower one of the parent or weld metal yield stresses acc. to SINTAP    |

**Abbreviations**

|          |  |
|----------|--|
| API      | American Petroleum Institute   |
| ASME     | American Society of Mechanical Engineers                                 |
| BWR      | Boiling Water Reactor  |
| CGR      | Crack Growth Rate  |
| DOF      | Degree Of Freedom  |
| EFPY     | Effective Full Power Year  |
| FEA      | Finite Element Analysis  |
| FEM      | Finite Element Method  |
| HAZ      | Heat affected zone   |
| IGSCC    | Intergranular stress corrosion cracking                                  |
| IWM      | Fraunhofer-Institut für Werkstoffmechanik                                |
| LC       | Load cycle   |
| LWR      | Light Water Reactor  |
| MIG      | Metal Inert Gas welding  |
| NPP      | Nuclear Power Plant  |
| PWHT     | Post Weld Heat Treatment   |
| PWR      | Pressurised Water Reactor  |
| RPV      | Reactor Pressure Vessel  |
| SAW      | Submerged Arc Welding  |
| SCC      | Stress Corrosion Cracking  |
| SDS      | Shut-down state  |
| SMAW     | Shielded Metal Arc Welding   |
| SO       | Start of operation   |
| SS       | Stainless Steel  |
| STS      | Static loading to steady state   |
| TIG      | Tungsten Inert Gas welding   |
| TVO      | Teollisuuden Voima Oy  |
| VTT      | Technical Research Centre of Finland                                     |
| VTTBESIT | fracture mechanics based analysis tool, which is partly developed at VTT |
| VYR      | State Nuclear Waste Management Fund (Valtion YdinjätöhuoltoRahasto)      |
| WRS      | Welding Residual Stress  |



# 1 Introduction and goal

This study concerns the welding process induced residual stresses in Nuclear Power Plant (NPP) reactor circuit component welds, and their practical inclusion in structural integrity analyses. The applicability of several commonly used welding residual stress (WRS) procedures for both Finite Element Method (FEM) based stress analyses and fracture mechanics based crack growth analyses of NPP reactor circuit component welds is assessed and discussed.

This study represents the results concerning the second year, i.e. 2008, of a research project spanning four years, i.e. 2007 – 2010. A literature study concerning various commonly used WRS procedures was carried out in the previous part of this research project during 2007, see ref. [1]. In that study seven commonly used WRS procedures were presented, and compared against each other in the light of a set of relatively simple application examples concerning NPP reactor circuit piping welds. The examined WRS procedures were: the ASME recommendations [2, 3], the British Standard BS 7910: 1999 [4], the R6 Method, Revision 4 [5], the SAQ handbook [6], the SINTAP Procedure [7, 8], the API 579 Procedure [9] and the FITNET Procedure [10]. The covered WRS types in ref. [1] were as-welded state, after Post Weld Heat Treatment (PWHT) and after repair. Besides the ASME recommendations [2, 3], the other six of the above mentioned procedures provide a compendium of fitness-for-service procedures for assessment of integrity of structures/components in general, covering not only NPP components, but also those in other energy facilities as well as in process and petrochemical industries. The present study continues the work of the previous part of the project. Here the emphasis is on more advanced numerical simulation of WRS distributions in a FEM model of a reactor circuit component, the selected type of which is a safe-end connecting to a nozzle and pipe. In particular, it is examined how to simulate with FEM the WRS distributions in one of the main joining welds concerning the analysed component assembly. Of the above mentioned WRS procedures the most suitable one with which to calculate the original as-welded state WRSs is selected first. Then this WRS procedure is applied to certain NPP reactor circuit components in ensuing FEM analyses. The capabilities and possibilities of advanced FEM analysis codes allowing 2D and 3D elastic-plastic analyses, e.g. Abaqus [11, 12], to simulate the WRSs are also discussed.

The goal of the work here is to study via numerical simulations how the WRSs alter over the years in plant operation in primary circuit component welds (e.g. to see if and how much they decrease), mainly due to various typical/anticipated transient load cases. When having such stress results, it is then examined what is their impact to the corresponding simulated crack growth rates. In the latter analyses a fracture mechanics based analysis tool is used. Especially when a NPP has been in operation for some decades, it could be assumed that the WRSs have relieved at least to some extent due to typical anticipated and repeated mechanical loads. On the other hand, the operational temperature of Finnish Boiling Water Reactor (BWR) units is not high enough for considerable time dependent stress relieving caused by creep to take place.

After this introductory chapter, the characteristics of the relatively high WRSs are presented and discussed in Chapter 2, together with conditions/treatments that can relax them.

The selection of the most suitable WRS procedure for calculation of the original as-welded state WRSs to be used in the numerical simulations carried out with a FEM code is presented



in Chapter 3. The scope of the candidate WRS procedures is limited to the above mentioned seven, as they seem to be the most reliable and applicable ones of the commonly used procedures presently available.

Numerical FEM simulations of WRSs in the selected primary circuit component in a Boiling Water Reactor (BWR) unit are described in Chapter 4. This includes a description of the needed analysis input data, of the prepared FEM model, and finally of the analysis results. The analyses cover a loading history starting with the system pressure test following with more than ten mechanical loading events.

Chapter 5 presents the crack growth analyses performed with a fracture mechanics based analysis tool. This includes a description of the needed analysis input data, of the used analysis tool, and finally of the analysis results. Here two cases are considered: the first one with WRSs kept in the level of as-welded state through the analysis, and the second one with considering the altering of the WRSs as a function of experienced load transients, as taken from the results of FEM simulations presented in Chapter 4.

Finally, summary and conclusions of the whole study as well as suggestions for further research are presented in Chapter 6.

## 2 Brief introduction to WRSs and their relieving

### 2.1 Introduction to WRSs

Assessment of the structural integrity of critical components and structures in NPPs is of remarkable importance for safe operation. When assessing the structural integrity of a component, both the loading and the load-carrying capacity are determined. The WRSs are included in the analysis on either the loading or capacity side, depending on the design strategy.

Since WRSs with various magnitudes and distributions are present in virtually all structurally engineered components, there is a demand for accurate assessment of the WRS distributions, especially in critical components. The residual stress distributions present in a structure are the result of the manufacturing history and the elastic-plastic properties of the structure. The former referring to the mechanical and thermal processes executed during the whole production sequence and the latter to the elastic-plastic behaviour of the structure. Because the elastic-plastic properties influence the severity and distribution of the WRSs, it follows that a structure comprised of several materials will experience the development of the WRSs in a completely different way than one made of a single material.

Depending on the importance of the WRSs, different approaches have been introduced for the assessment of the structural integrity. In structures where the effect of the WRSs on the performance is limited or small, the assessment of the WRSs is of less importance. On the other hand, in the structures where their integrity is of remarkable importance for their reliability, such as NPP primary circuit components, a thorough and accurate assessment of the WRS state is of primary concern. NPPs are typically concerned with manufacturing and managing components which are strongly regulated by national and/or international technical guidelines, standards and design codes to ensure reliable operation.

WRSs are defined as static mechanical stresses that are present in a thermodynamically (and mechanically) closed system of equilibrium. In a more general way, WRSs are mechanical stresses that exist in a component without any external applied mechanical or thermal loads. A direct consequence of the definition is that all internal forces and moments resulting from the WRSs of a system are in mechanical equilibrium. The size of the considered system determines the type of the WRSs that are assessable.

Another consequence of the above mentioned definition is that the internal stresses induced by thermal transients are outside the scope of the WRSs, as they do not represent closed systems. Such load transients are typical for uneven cooling during heat treatments and thermal in-service loads. However, the thermal transients can induce WRSs, when the yield strength is exceeded locally and plastic flow occurs.

The mechanical properties that govern the formation of WRSs are primarily the modulus of elasticity and the strain hardening coefficient. In the case of a work hardening material the WRSs are completely different than for a work softening material. Thus, a mismatch in strain

hardening capabilities in adjoining materials, with otherwise similar elastic properties, induces local plastic deformation in the weaker material.

Manufacturing of welded structures in NPPs is carried out with traditional methods for which there is considerable welding experience. The methods are Shielded Metal Arc Welding (SMAW), Tungsten Inert Gas welding (TIG) and Submerged Arc Welding (SAW). However, Metal Inert Gas welding (MIG) is generally not used due to a higher risk for lack of fusion. Manufacturing of clad structures is a time consuming process, and therefore it is mostly done with SAW. Other methods have also been used, though less frequently. Butt welding of pipes, on the other hand, is made with TIG.

Regardless of the welding method used, the material properties of the welds and the structural materials affect the formation and distribution of WRSs. The resulting WRS state in a welded component is determined by welding related parameters and geometrical constraints. The former refers to the local shrinkage, quench and phase transformations resulting from the localised thermal cycle. The latter is dealt with through the unbalance in material properties of dissimilar metal welds, and the constraining effect of the surrounding structure. In NPP primary circuits there are typically several dissimilar joint welds.

The components of primary interest in NPPs often have a bi-metallic or dissimilar metal structure, where the mechanical properties of the joined materials are different, and thus add to the formation of the WRSs. However, in most cases NPP primary circuit welds are similar, i.e. same materials are joined in a weld.

## 2.2 On the conditions/treatments that relieve WRSs in NPP components

In the assessment of the WRS distributions in NPP components, the possible relaxation of them by post processing or during service operation has to be taken into account. It is a generally known fact that there are three primary sources for WRS redistribution or relaxation. These are described in the following

The first source of WRS relaxation is related to irradiation effects, which have been studied for several stainless steels and nickel-base alloys. The results showed that exposure to a high neutron fluency level corresponding to over ten Effective Full Power Years (EFPY) causes the WRSs to relax by 30 % [16].

The second source of WRS relaxation is due to thermal effects. It is well known that prolonged holding or operating times at elevated temperatures causes WRSs to relax. At the BWR operating temperature of 286 °C the time dependent relaxation of WRSs due to creep is small and further relatively small compared to irradiation related relaxation. Even though the operating temperature of a Pressurised Water Reactor (PWR) is approximately 50 °C higher than that of a BWR, the thermal relaxation effects still remain small. Relaxation of the WRSs requires higher temperatures, where the yield strength drops below the WRS and plastic flow occurs. A controlled reduction in the magnitude of the WRSs is obtained when applying a PWHT to the component. The treatment time and temperature are primarily determined by the involved alloys.

In the third case, a static or dynamic mechanical load is applied to cause local plastic yielding, which redistributes the WRSs. Reference [17] presents a study on the effect of static and

spectrum loading on the WRSs. As the location of the highest tensile WRSs, i.e. the weld toe, is close to the yield point of the metal, a tensile load causes the weld toe stress to exceed the yield point and local plastic deformation takes place. To compensate for the reduction in load carrying capacity of the weld toe, the surrounding stress field changes to accommodate the load increase. As the applied load is removed, the WRS distribution has been altered and the highest tensile stresses have been reduced.

Based on the measurement data concerning the relaxation of the WRSs, analysis models have been developed to capture this effect. In this study one of the main objects is to examine with numerical simulations how repeated mechanical loads affect the local WRS maximum and overall levels.

### 3 On the selection of suitable WRS assessment procedure for numerical simulations

#### 3.1 Applicability of commonly used WRS assessment procedures for numerical simulations

Here the considered WRS procedures are: the ASME recommendations [2, 3], the British Standard BS 7910: 1999 [4], the R6 Method, Revision 4 [5], the SAQ handbook [6], the SINTAP Procedure [7, 8], the API 579 Procedure [9] and the FITNET Procedure [10]. As mentioned earlier, the same WRS procedures were examined in the previous part of the project, see ref. [1]. The covered WRS type here is as-welded state. The WRS definitions in the mentioned procedures are based both on the available experimental data and FEM analysis results. In some older ones of the mentioned WRS procedures, uniform distributions have conservatively been defined to WRSs for some cases due to lack of data, e.g. those given for parallel to weld for austenitic stainless steel for pipe-to-pipe welds in ASME recommendations [2, 3].

The published experimental WRS data have a substantial scatter. Consequently the defined WRS distributions have been developed as tensile upper bound solutions based on the data. However, according to [18, 19, 20, 21], this approach not only lacks consistency for the same type of joints and welding parameters, but can either significantly overestimate the WRS level in some cases, or underestimate it in others.

Over the last decade or so, WRSs have received increasing attention in the pressure vessel and piping research community. The driving force for this interest can be attributed to the fact that application of modern structural integrity assessment procedures for defective welded components, e.g., the British Standard BS 7910: 1999 [4], R6 Method, Revision 4 [5], SINTAP Procedure [7, 8], API 579 Procedure [9] and FITNET Procedure [10], require considerably more input data on the WRS state to give a more realistic assessment. The conventional approach for characterising a WRS profile has been to adopt a tensile upper bound solution, as mentioned above. All WRS procedures covered here base their definitions on material yield strength, so that typically the maximum absolute WRS values are nearly at yield strength, usually acting at weld inner and outer surfaces. The variation of the yield stress values within the typical operational temperature range in Light Water Reactor (LWR) NPP piping systems, being approximately from 20 to 330 °C, is of the scale of 10 %. For austenitic NPP piping stainless steels (SSs) the stress values at 1.0 % strain should most often be used for yield strength, whereas for corresponding ferritic SSs the stress values at 0.2 % strain should be used, respectively.

The mentioned seven WRS procedures provide a range of approaches to define the WRS distributions. In older WRS procedures, such as ASME recommendations [2, 3], only one approach in the form of a few simple functions is given, whereas in the more recent WRS procedures, such as R6 Method Rev. 4 [5] and FITNET Procedure [10], a selection of levels for defining WRSs are presented, ranging from coarse level 1 definitions giving single values, to level 2 with WRS definitions as analytical functions, to subtle and computationally

laborious level 3 approaches, requiring e.g. the use of advanced non-linear 3D FEM analysis tools. Depending on the needed accuracy and available resources, one can choose which WRS procedure and level to apply. In general, the WRS distributions are defined in all of the mentioned seven procedures also (or only) with analytic functions, such as polynomials and exponent function. On the behalf of the more recent WRS procedures, these correspond to level 2 definitions. Separate definitions are typically given for austenitic and ferritic SS materials, weld types and weld wall thickness ranges. Also, overall validity ranges are given in most procedures for WRS definitions, as a function of e.g. weld wall thickness and yield strength.

One unfortunate departure from realism in case of some of the more recent WRS procedures, e.g. R6 Method Rev. 4 and FITNET, is that in the transverse to weld direction the WRSs are mostly not self-balancing. While making local crack growth calculations with a fracture mechanics based analysis tool this feature may not pose remarkable problems, but in case of corresponding 3D FEM analyses it is quite the other way around, as in order to achieve equilibrium FEM automatically modifies the WRSs towards self-balanced distributions over the component model walls, and thus the original WRS distributions are not maintained.

In the light of the WRS analysis results presented in ref. [13], only ASME recommendations [2, 3] and SINTAP procedure [7, 8] in all cases, and SAQ handbook in most cases [6], give as-welded state WRS distributions that are self-balancing in the transverse to weld direction. Of them the least over conservative WRS procedure appears to be SINTAP.

Based on what is explained above in this section, the SINTAP procedure [7, 8] is selected to be used for defining the as-welded state WRSs to be used in the FEM simulations in this study.

## 3.2 WRSs according to SINTAP procedure

SINTAP; Structural Integrity Assessment Procedures for European Industry [7, 8] presents definitions for WRSs applicable to NPP reactor circuit component welds of several types, including circumferential piping welds and repair welds. SINTAP also contains equations for considering PWHT.

The stress profiles are normalised to the yield stress  $\sigma_y$  [MPa] ( $\sigma_y$  = yield or 0.2 % proof stress) of the weld metal or parent metal. The parameter,  $\sigma_y$ , refers mainly to the yield stress of the weld,  $\sigma_{yw}$  [MPa], for longitudinal WRSs except for a few cases. For transverse WRSs,  $\sigma_y$  is the lower of the weld metal  $\sigma_{yw}$  and the parent metal yield stress  $\sigma_{yp}$  [MPa], except when there is a defect of the type listed below:

1. Defect in repair weld,
2. Defect at weld intersection,
3. Shallow defect.

Here,  $\sigma_y$  refers to the greater yield stress of the parent metal or weld metal. For austenitic SSs, the high work hardening after the beginning of the plastic deformation, results in a large variability of the material properties. In this case, the yield stress  $\sigma_y$  is defined as the 1.0 % proof stress. To a first approximation:  $\sigma_y (\epsilon = 1.0 \%) \approx 1.5 \cdot \sigma_y (\epsilon = 0.2 \%)$ .

If the defect is being assessed in an area of constant and uniform temperature, the appropriate value of  $\sigma_y$  is the yield stress at the temperature of the assessment. If the temperature varies

within the defective area, then the appropriate value of  $\sigma_y$  is the maximum value of yield stress which usually corresponds to that at the minimum temperature recorded.

### Circumferential WRSs in piping butt welds

The circumferential WRS distribution for ferritic and austenitic steel pipe butt welds is represented conservatively by a linear profile defined by a stress equal to yield stress,  $\sigma_R^{L,O}$ , at the outer surface and longitudinal residual stress,  $\sigma_R^{L,B}$ , at the bore, where longitudinal is in weld coordinates which stands for circumferential in piping coordinates, see Figure 3.2-1. The equations are:

$$\sigma_R^{L,O} = \sigma_{yw} \quad (3.2-1a)$$

$$\sigma_R^{L,B} = A_b \cdot \sigma_{yw} \quad (3.2-1b)$$

where:

$$A_b = 1, \quad \text{for } 0 < t < 15 \text{ mm} \quad (3.2-1c)$$

$$A_b = 1 - 0.0143 \cdot (t - 15), \quad \text{for } 15 < t \leq 85 \text{ mm} \quad (3.2-1d)$$

$$A_b = 0, \quad \text{for } t > 85 \text{ mm} \quad (3.2-1e)$$

where  $\sigma_{yw}$  [MPa] is weld metal typical yield stress and  $t$  [mm] is wall thickness.

For a pipe wall thickness of less than 15 mm, a through thickness tensile yield stress is obtained. The tensile stress at the bore decreases with increasing pipe thickness to a value of zero for a pipe thickness of approximately 85 mm.

### Axial WRSs in piping butt welds

No detailed profiles are proposed for surface axial WRSs because there are insufficient data available and because these stresses are geometry sensitive. In this case, a uniform stress  $\sigma_R^T$  equal to  $\sigma_y^*$ , the lower of the parent or weld metal yield stresses, should be considered.

Through thickness axial WRS distributions for ferritic and austenitic steel pipe butt welds are depicted in Figure 3.2-1.

For austenitic steels the through thickness WRS distribution depends, among other things, on the wall thickness.

The equations are:

$$\sigma_R^T = 1.219 \cdot \sigma_y^* \cdot \left( \frac{2 \cdot z}{t} - 1 \right), \quad \text{for } t \leq 7 \text{ mm} \quad (3.2-2a)$$

$$\sigma_R^T = (1.5884 - 0.05284 \cdot t) \cdot \sigma_y^* \cdot \left( \frac{2 \cdot z}{t} - 1 \right), \quad \text{for } 7 < t \leq 25 \text{ mm} \quad (3.2-2b)$$



$$\sigma_R^T = \sigma_R^{T,B} \cdot \left[ 0.27 - 0.91 \cdot (z/t) - 4.93 \cdot (z/t)^2 + 8.60 \cdot (z/t)^3 - 2.03 \cdot (z/t)^4 \right], \quad \text{for } t \geq 25 \text{ mm} \quad (3.2-2c)$$

where:

$$\sigma_R^{T,B}(R/t) = 0.118 \cdot \sigma_y^* \cdot (R/t), \quad \text{for } R/t < 8.5 \quad (3.2-2d)$$

$$\sigma_R^{T,B}(R/t) = 1.0 \cdot \sigma_y^*, \quad \text{for } R/t > 8.5 \quad (3.2-2e)$$

where  $z$  [mm] is the radial coordinate through wall having origin at the outer pipe surface,  $t$  [mm] is the wall thickness,  $\sigma_y^*$  [MPa] is the lower of the parent or weld metal yield stresses and  $R$  [mm] is the outer pipe radius.

A few comments concerning SINTAP documentation are presented in the following.

Equations (3.2-2d) and (3.2-2e) for  $\sigma_R^{T,B}$  values are not presented in the main SINTAP report, i.e. reference [7], instead they had to be taken from the related reference [8]. However, in that reference the mentioned equations are presented without factor  $\sigma_y^*$ , which has been added here by the author of this report. This was carried out to keep the equation (3.2-2c) for  $\sigma_R^T$  in line with the corresponding equations (3.2-2a) and (3.2-2b) for the same WRS component for smaller wall thicknesses, which both do contain the factor  $\sigma_y^*$ . Also, without the addition of factor  $\sigma_y^*$  to equations (3.2-2d) and (3.2-2e), the equation (3.2-2c) would have given results with erroneous physical dimension, and the resulting values for wall thickness of e.g. 26 mm varied between zero to one, which are unrealistically low WRS result values, for details see [1].

Also, the presentation of the equation that in this report is the equation (3.2-2c) had some deviations in their presentations according to references [7] and [8]. Namely, according to reference [7] the signs in front of the four latter terms inside the outer parenthesis in the right hand side are, from left to right: “+”, “-“, “+” and “-“, whereas in reference they are: “-“, “-“, “+” and “-“, respectively. When applying the mentioned equation for wall thickness of 26 mm, the resulting values varied from 350 MPa in the inner surface to 30 MPa in the outer surface according to reference [7], and from 125 MPa to 30 MPa in according to reference [8], respectively, for details see [1]. The latter results were much better in line when compared to corresponding results calculated with the equations (3.2-2a) and (3.2-2b) for the same WRS component for smaller wall thicknesses, and thus this form for the mentioned equation was used, i.e. equation (3.2-2c) here.

For ferritic steels the WRS distribution depends, among other things, on the heat input and the wall thickness.

For high heat input values, i.e. for  $[(q/v)/t] > 60 \text{ J/mm}^2$ , the following equation is employed:

$$\sigma_R^T = \sigma_R^{T,O} \cdot \cos[(\pi \cdot z)/t] \quad (3.2-3a)$$

where:

$$\sigma_R^{T,O} / \sigma_y^* = -1.0 \quad (3.2-3b)$$

and  $z$  [mm] is the radial coordinate through wall with origin in the outer surface.

For low heat input values, i.e. for  $[(q/v)/t] < 60 \text{ J/mm}^2$ , the following equation is employed:

$$\sigma_R^T = \sigma_R^{T,O} \cdot \left[ 1.0 - 3.29 \cdot (z/t) - 26.09 \cdot (z/t)^2 + 73.16 \cdot (z/t)^3 - 45.72 \cdot (z/t)^4 \right] \quad (3.2-3c)$$

where:

$$\sigma_R^{T,O} / \sigma_y^* = -0.5 - 0.0083 \cdot [(q \cdot v)/t] \quad (3.2-3d)$$

Here the left side of equation (3.2-3b) was divided with  $\sigma_y^*$  as compared to how the corresponding definition is presented in references [7] and [8]. This was due to same reasons as the corresponding modification performed to equations (3.2-2d) and (3.2-2e), for details see [1].

### WRSs in repair weld centre-line

The longitudinal residual stress distribution for ferritic and austenitic repair welds is presented in Figure 3.2-2. The surface longitudinal WRS distributions apply both to ferritic and austenitic steels, while all other repair WRS distributions apply to ferritic steels only. When the repair weld is short the through thickness WRS distributions in both longitudinal and transverse directions are identical. The distribution for the surface transverse WRS distribution should only be used for a full length repair weld.

For through thickness WRSs, the highest of the yield stresses of the parent plate material, original weld material and repair weld material should be used. Below the repair the WRSs reduce linearly with distance to zero at a distance  $z_0$  below the root of the repair. Parameter  $z_0$  is related to the heat input of the repair weld and is defined in the following.

The transverse and longitudinal WRS distributions in repair welds should be considered to be of yield magnitude throughout the depth of the repair. For part depth repairs of depth  $z_r$ , the WRSs may be assumed to decrease from yield magnitude at the bottom of the repair, where  $z_0$  is defined in the following way:

$$z_0 = \sqrt{\frac{122}{\sigma_y} \cdot \frac{q}{v}}, \quad (3.2-4a)$$

$$\text{for } z \leq z_r: \quad \sigma_R^T = \sigma_R^L = \sigma_Y \quad (3.2-4b)$$

$$\text{for } z_r \leq z \leq (z_r + z_0): \quad \sigma_L^T = \sigma_R^L = \sigma_Y \cdot \left( \frac{z_0 + z_r - z}{z_0} \right) \quad (3.2-4c)$$

$$\text{for } z \geq (z_r + z_0): \quad \sigma_R^T = \sigma_R^L = 0 \quad (3.2-4d)$$

where  $z_0$  [mm] is measured from the face of the component from which the repair was made,  $\sigma_y$  [MPa] is the yield or 0.2 % proof strength of parent metal,  $q$  [J/sec] is the weld arc power and  $v$  [mm/sec] is the weld travel speed.

### **Effect of PWHT to WRSs**

The effectiveness of PWHT on the relief of WRSs depends on several characteristics, e.g. geometry of the component, base and weld material strength properties, PWHT temperature and duration.

Invariably, PWHT does not reduce the WRSs to zero, the exact value depending on the complex interactions of the several involved characteristics. Experimental and modelling work supports the following recommendations for the effect of PWHT to be taken as:

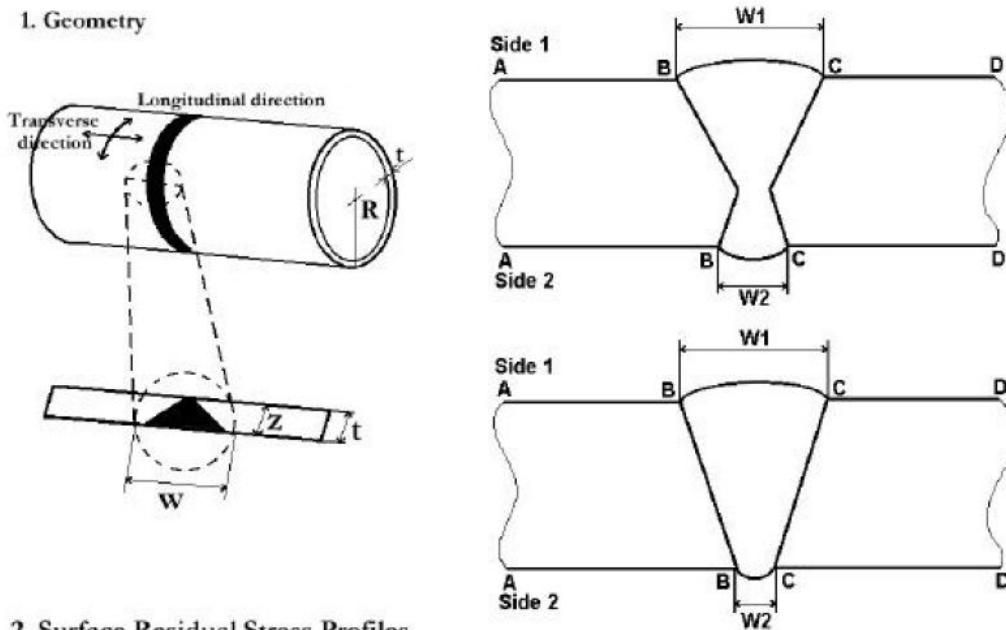
- 30 % of the yield stress of the material in which the flaw lies for longitudinal WRSs
- 20 % of the lower of the yield stress of the parent plate and weld material for transverse WRSs

Alternative values may be used where modelling or experimental work is available for such justification.

**PIPE BUTT WELDS**

Material : Ferritic, Austenitic steels and Aluminium

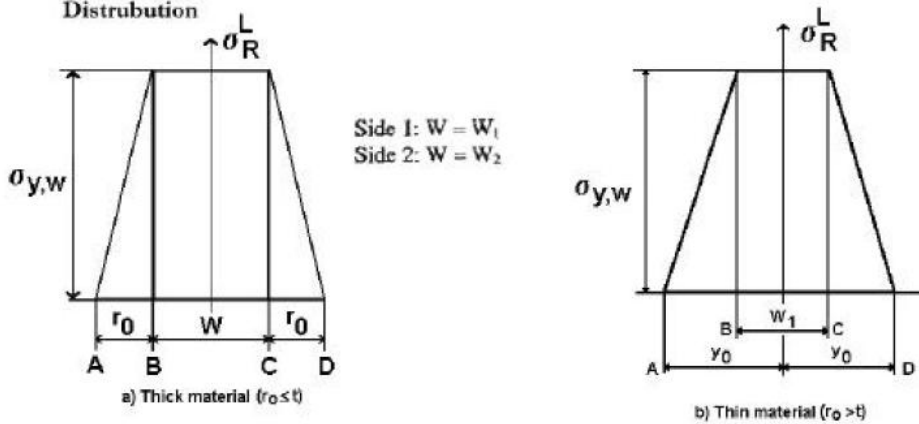
1. Geometry



2. Surface Residual Stress Profiles

2.1 Longitudinal Residual Stress,  $\sigma_R^L$  ( fig 3a )

Distribution



(For definitions of  $r_0, y_0$ , see Appendix 1)

2.2 Transverse Residual Stress,  $\sigma_R^T$  ( fig 3c )

Use uniform  $\sigma_R^T = \sigma y^*$

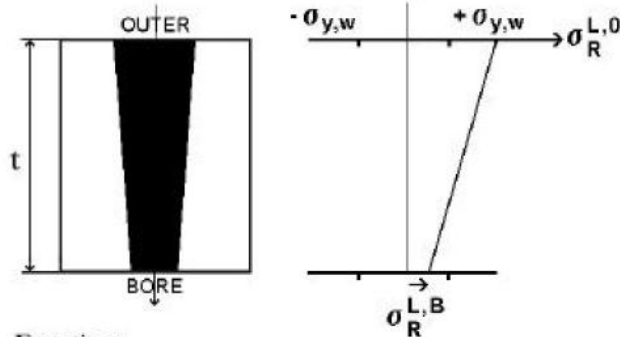
$$\sigma y^* = \text{lower of } (\sigma_{yw}, \sigma_{yp})$$

Figure 3.2-1a. The longitudinal and transverse surface WRS distributions for ferritic and austenitic steel pipe butt welds [7]. Here longitudinal and transverse stand for circumferential and axial in pipe coordinates, and  $r_0$  [mm] is the radius of the yield zone, respectively.

### 3. Through Thickness Residual Stress Profiles

#### 3.1 Longitudinal Residual Stress, $\sigma_L^R$

Distribution



Equations

$$\sigma_R^{L,B} = Ab \sigma_{y,w}$$

Where:  $Ab = 1$

$$Ab = 1 - 0.0143 (t-15)$$

$$Ab = 0$$

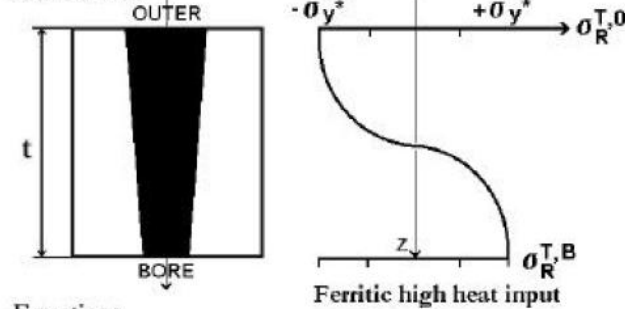
$$0 < t \leq 15 \text{ mm}$$

$$15 \text{ mm} < t \leq 85 \text{ mm}$$

$$t > 85 \text{ mm}$$

#### 3.2 Transverse Residual Stress, $\sigma_R^T$

Distribution



Equations

FERRITIC STEELS

For Low heat inputs  $(q/v)t < 60 \text{ J/mm}^2$  and  $\sigma_R^{T,0}/\sigma_{y^*} = -0.5 - 0.0083(q/v)t$

$$\sigma_R^T = \sigma_R^{T,0} (1.0 - 3.29(z/t) - 26.09(z/t)^2 + 73.16(z/t)^3 - 45.72(z/t)^4)$$

For High heat inputs  $(q/v)t > 60 \text{ J/mm}^2$  and  $\sigma_R^{T,0} = -1.0$

$$\sigma_R^T = \sigma_R^{T,0} \cos(\pi z/t); \text{ z measured from outer surface}$$

AUSTENITIC STEELS

$t < 25 \text{ mm}$

$$t \leq 7 \text{ mm} \quad \sigma_R^T = 1.219 \sigma_{y^*} \left[ \frac{2z}{t} - 1 \right]$$

$$7 \text{ mm} < t \leq 25 \text{ mm} \quad \sigma_R^T = (1.5884 - 0.05284 t) \sigma_{y^*} \left[ \frac{2z}{t} - 1 \right]$$

$t \geq 25 \text{ mm}$

$$\sigma_R^T = \sigma_R^{T,B} (0.27 - 0.91(z/t) - 4.93(z/t)^2 + 8.60(z/t)^3 - 2.03(z/t)^4)$$

For definition of  $\sigma_R^{T,B}$  see paragraph 5.3.2

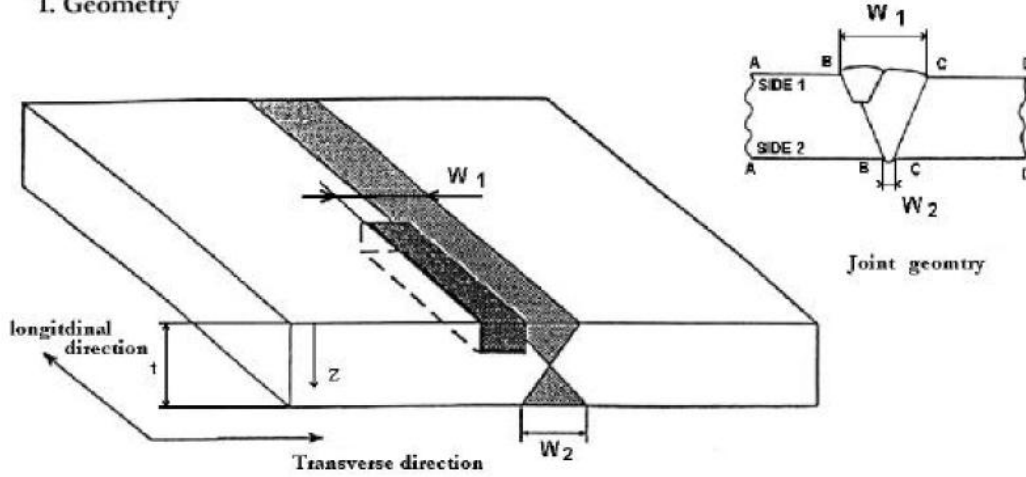
$$\sigma_{y^*} = \text{lower of } (\sigma_{yw}, \sigma_{yp})$$

Figure 3.2-1b. The longitudinal and transverse through wall WRS distributions for ferritic and austenitic steel pipe butt welds [7]. Here longitudinal and transverse stand for circumferential and axial in pipe coordinates, and  $r_0$  [mm] is the radius of the yield zone, respectively.

**REPAIR WELDS**

Material: Ferritic austenitic steels and Aluminum (7a)  
 Ferritic steels (7b),(7c),(7d)

**1. Geometry**



**2. Surface Residual Stress Profiles**

**2.1 Longitudinal Residual Stress,  $\sigma_R^L$  (fig 7a)**

Distribution

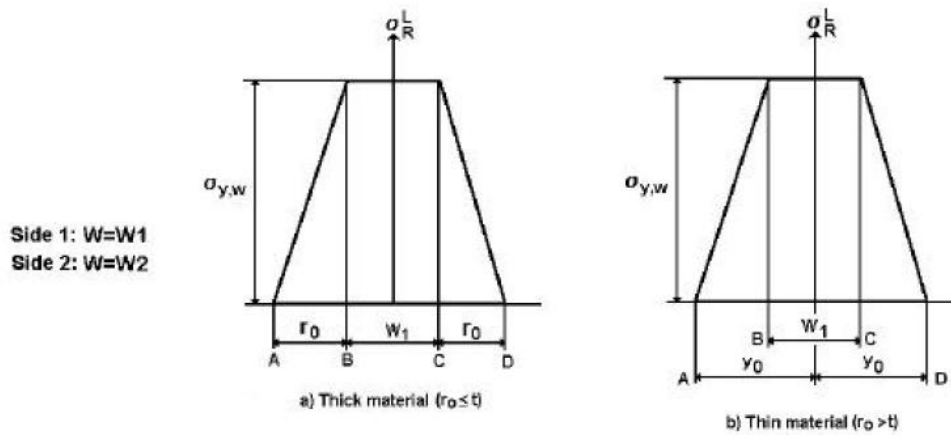
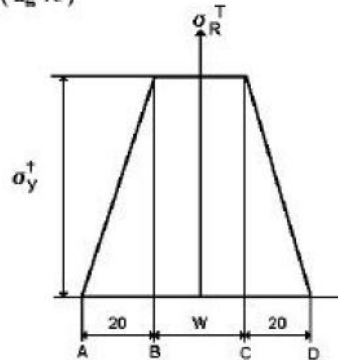


Figure 3.2-2a. The longitudinal surface WRS distributions for ferritic and austenitic steel repair welds [7], and  $r_0$  [mm] is the radius of the yield zone, respectively.

2.2 Transverse Residual Stress,  $\sigma_R^T$  ( fig 7e )  
Distrubution

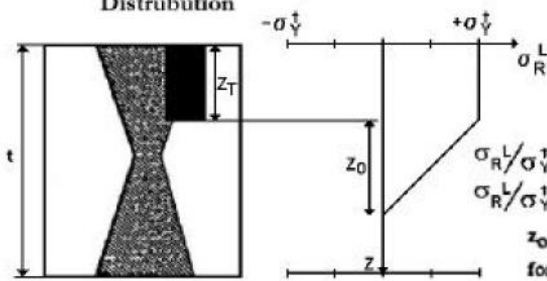
Side 1:  $W=W1$   
Side 2:  $W=W2$



3. Through-thickness Residual Stress Profiles

3.1 Longitudinal Residual Stress ( fig 7b )

Distrubution

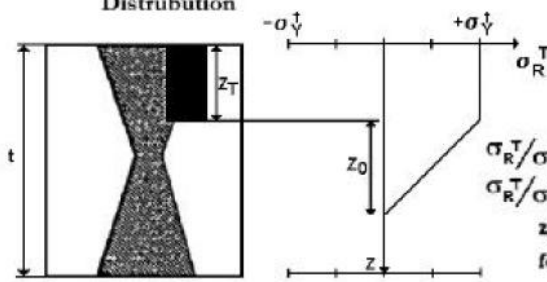


Equations

$$\begin{aligned} \sigma_R^L / \sigma_y^+ (z/t) &= 1.0 \text{ for } z < z_T \text{ where } z_T \text{ is the depth of the repair} \\ \sigma_R^L / \sigma_y^+ (z/t) &= (z_0 + z_T - z) / z_0 \text{ where } z_0 \text{ is given by} \\ z_0 &= \sqrt{(122(q/v) / \sigma_y)} \text{ where } (q/v) \text{ is in J/mm and } \sigma_y^+ \text{ is in MPa} \\ \text{for } z > z_0 \quad \sigma_R^L / \sigma_y^+ (z/t) &= 0.0 \end{aligned}$$

3.2 Transverse Residual Stress ( fig 7d )

Distrubution



Equations

$$\begin{aligned} \sigma_R^T / \sigma_y^+ (z/t) &= 1.0 \text{ for } z < z_T \text{ where } z_T \text{ is the depth of the repair} \\ \sigma_R^T / \sigma_y^+ (z/t) &= (z_0 + z_T - z) / z_0 \text{ where } z_0 \text{ is given by} \\ z_0 &= \sqrt{(122(q/v) / \sigma_y)} \text{ where } (q/v) \text{ is in J/mm and } \sigma_y^+ \text{ is in MPa} \\ \text{for } z > z_0 \quad \sigma_R^T / \sigma_y^+ (z/t) &= 0.0 \end{aligned}$$

$$\sigma_y^+ = \text{greater of (original or repair weld yield stress)}$$

Figure 3.2-2b. The transverse surface WRS distribution as well as longitudinal and transverse through wall WRS distributions for ferritic repair welds [7].



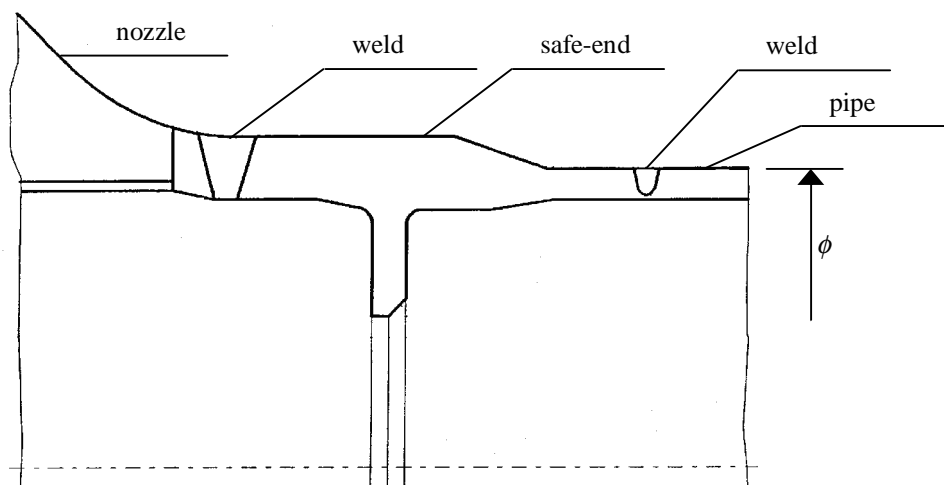
## 4 Numerical simulations of WRSs in a BWR primary circuit component

The numerical simulations concerning the selected BWR primary circuit component, or rather certain components joined with welds, are presented in this chapter. The type of the selected component assembly is a safe-end connecting to a nozzle and pipe, resembling those that connect the feed water system to the Reactor Pressure Vessel (RPV) in BWR units. In particular, it is examined how to simulate with FEM the WRS distributions in one of the main welds connecting these components. As explained in Chapter 3, the SINTAP procedure [7, 8] is selected for defining the as-welded state WRSs to be used in the FEM simulations in this study. The analysis tool selected for numerical simulations is Abaqus [11, 12], which is an advanced FEM analysis code, allowing time dependent 2D and 3D elastic-plastic analyses. The capabilities and possibilities of FEM codes to simulate the WRSs are also discussed. In this chapter, a description of the needed analysis input data including geometry, material properties and loads, is presented first. The applied time dependent load cases, of which a loading history starting with the system pressure test and following with more than ten mechanical load events is formed, are described next. Then the prepared FEM model is presented, together with the associated boundary conditions. This follows with a presentation of the performed heat transfer and stress/strain FEM simulations. Finally, the WRS simulation results are presented.

### 4.1 Analysis input data

#### 4.1.1 Geometry

The general geometry of the analysed BWR primary circuit components is presented in the following Figures 4.1.1-1 and 4.1.1-2.



*Figure 4.1.1-1. The overall geometry of the safe-end connecting to a nozzle and pipe, resembling those that connect the feed water system to the RPV in BWR units; horizontal section of the components at the level of their common symmetry axis. The outer diameter  $\phi$  is of the scale of a few hundred mm.*

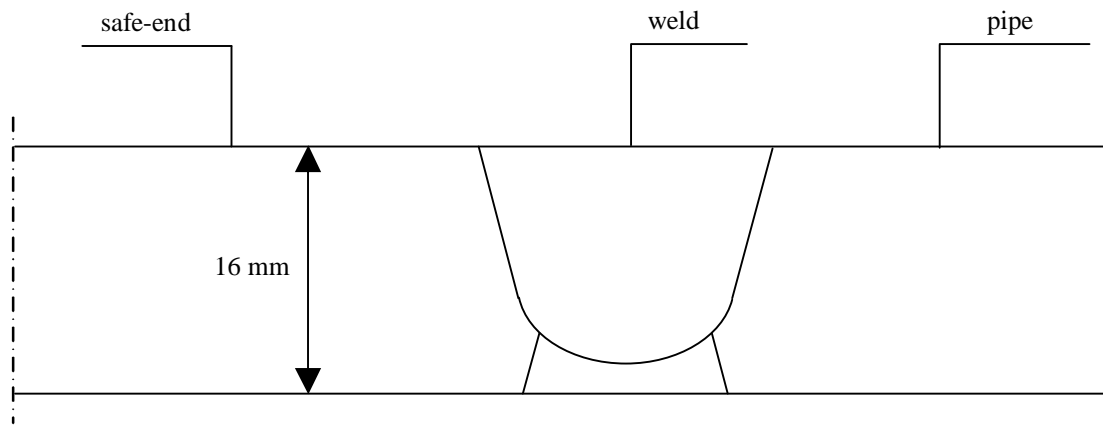


Figure 4.1.1-2. Geometry detail of the analysed safe-end/pipe joint weld, for its location see Figure 4.1.1-1.

#### 4.1.2 Material properties

The material types of the components covered in the numerical simulations are listed in Table 4.1.2-1.

Table 4.1.2-1. Material regions of the analysed nozzle, safe-end and pipe, together with joining welds.

| Component            | Location      | Material Type            |
|----------------------|---------------|--------------------------|
| Nozzle               | Base material | Ferritic steel           |
| Nozzle/safe-end weld | Beads & root  | Austenitic weld material |
| Safe-end             | Base material | Austenitic SS            |
| Safe-end/pipe weld   | Beads & root  | Austenitic weld material |
| Pipe                 | Base material | Austenitic SS            |

The material properties of the austenitic SSs considered in the FEM analyses are presented in the following in Tables 4.1.2-2 to 4.1.2-6.

Table 4.1.2-2. Strength properties of the austenitic SS safe-end material and austenitic weld material, the values were taken from ref. [14].

| Temperature<br>$T$ [°C] | Yield strength<br>$S_y$ [MPa] | Design stress<br>$S_m$ [MPa] | Tensile strength<br>$S_u$ [MPa] |
|-------------------------|-------------------------------|------------------------------|---------------------------------|
| 21                      | 241                           | 137                          | 586                             |
| 93                      | 229                           | 137                          | 586                             |
| 149                     | 223                           | 137                          | 586                             |
| 204                     | 220                           | 137                          | 586                             |
| 260                     | 220                           | 137                          | 586                             |
| 286                     | 220                           | 137                          | 586                             |
| 316                     | 220                           | 137                          | 586                             |

Table 4.1.2-3. Strength properties of the austenitic SS pipe material, the values were taken from ref. [14].

| Temperature<br>$T$ [°C] | Yield strength<br>$S_y$ [MPa] | Design stress<br>$S_m$ [MPa] | Tensile strength<br>$S_u$ [MPa] |
|-------------------------|-------------------------------|------------------------------|---------------------------------|
| 20                      | 172                           | 115                          | 483                             |
| 100                     | 146                           | 115                          | 452                             |
| 150                     | 132                           | 115                          | 421                             |
| 200                     | 121                           | 110                          | 406                             |
| 250                     | 114                           | 103                          | 398                             |
| 275                     | 111                           |                              |                                 |
| 300                     | 108                           | 97.7                         | 393                             |

Table 4.1.2-4. Some mechanical properties of the austenitic SS safe-end material and austenitic weld material, the values were taken from ref. [14].

| Temperature<br>$T$ [°C] | Elastic modulus<br>$E$ [GPa] | Thermal conductivity<br>$\lambda$ [W/m°C] | Specific heat<br>$c$ [J/kg°C] | Coefficient of thermal expansion<br>$\alpha_T \cdot 10^{-06}$ [1/°C] |
|-------------------------|------------------------------|---|-------------------------------|--|
| 21                      | 213.7                        | 14.9                                      | 451                           | 12.2   |
| 38                      |                              | 15.1                                      | 456                           | 12.4   |
| 66                      |                              | 15.4                                      | 464                           | 12.7   |
| 93                      | 208.2                        | 15.8                                      | 471                           | 13.0   |
| 121                     |                              | 16.1                                      | 475                           | 13.2   |
| 149                     | 206.2                        | 16.6                                      | 485                           | 13.3   |
| 177                     |                              | 17.0                                      | 486                           | 13.5   |
| 204                     | 203.4                        | 17.5                                      | 494                           | 13.6   |
| 232                     |                              | 17.8                                      | 495                           | 13.8   |
| 260                     | 199.9                        | 18.3                                      | 501                           | 13.9   |
| 288                     |                              | 18.7                                      | 507                           | 14.0   |
| 316                     | 197.9                        | 19.2                                      | 515                           | 14.1   |

Table 4.1.2-5. Some mechanical properties of the austenitic SS pipe material, the values were taken from ref. [14].

| Temperature<br>$T$ [°C] | Elastic modulus<br>$E$ [GPa] | Thermal conductivity<br>$\lambda$ [W/m°C] | Specific heat<br>$c$ [J/kg°C] | Coefficient of thermal expansion<br>$\alpha_T \cdot 10^{-06}$ [1/°C] |
|-------------------------|------------------------------|---|-------------------------------|--|
| 21                      | 195                          | 14.9                                      | 484                           | 15.2   |
| 38                      |                              | 15.1                                      | 486                           | 15.4   |
| 66                      |                              | 15.6                                      | 496                           | 15.6   |
| 93                      | 190                          | 16.1                                      | 506                           | 15.8   |
| 121                     |                              | 16.6                                      | 516                           | 16.0   |
| 149                     | 186                          | 17.0                                      | 520                           | 16.2   |
| 177                     |                              | 17.5                                      | 529                           | 16.4   |
| 204                     | 183                          | 18.0                                      | 535                           | 16.5   |
| 232                     |                              | 18.3                                      | 539                           | 16.7   |
| 260                     | 178                          | 18.9                                      | 544                           | 16.9   |
| 288                     |                              | 19.2                                      | 548                           | 17.0   |
| 316                     | 174                          | 19.6                                      | 551                           | 17.2   |

Table 4.1.2-6. Values of density and Poisson's coefficient for the considered materials, which values were taken from ref. [14].

| Material                        | Density<br>$\rho$ [kg/m <sup>3</sup> ] | Poisson's coefficient<br>$\nu$ [-] |
|---------------------------------|--|------------------------------------|
| austenitic SS safe-end material | 8430                                   | 0.3                                |
| austenitic SS pipe material     | 7850                                   | 0.3                                |

### 4.1.3 Loads

The stresses and strains acting in the analysed safe-end as well as connected nozzle and pipe are induced by various assumed load cases and types of loads. The transient and stationary load cases considered in the heat transfer and the stress/strain analyses are presented in the following. Also, the dead weights of the analysed components were considered, based on their dimensions and material densities.

#### System loads

The covered system load cases, i.e. those caused by plant process conditions and their variations, are presented in the following. These load cases consist both of anticipated load transients as well as of static loads.

As mentioned earlier, a history of anticipated load transients was analysed. This means that they were all included in a single analysis run in a realistic chronological order and separated from each other by static loading conditions long enough for steady state to take place. Thus the effect of structural memory, i.e. the effect to each present elastic-plastic stress/strain state of all earlier loads, was fully included. The considered load transients were also assembled in such a way that they form realistic load cycles. The definition here for a load cycle is such that as the values of the load parameters alter from their original reference state they must return to it for a full cycle to be complete. Here the considered load parameters are pressure, temperature and flow rate, and the considered reference state is the operational conditions, as the plant resides in that state for the most part of its operational lifetime. During some of the considered load transients the altering of the load parameters changes directions two or more times, thus forming sub-cycles with relatively low stress ranges, as a load event of cyclic type can be deemed to have occurred, when after two changes to opposite directions the load parameters reach again the values they had at the time instant of the first change. All cyclic load phenomena are on the other hand more associated with material fatigue. However, in the present study all details and characteristics of each considered load transient were included in the time dependent non-linear FEM analyses.

The considered load transients are as follows:

- 1) System pressure test,
- 2) Cold shut-down,
- 3) Cold start-up,
- 4) Feed water line opened at 320 kg/s,
- 5) Reactor scram, during normal operation with normal feed water flow,
- 6) Feed water line closed at 320 kg/s,
- 7) A – isolation.

During load transients 2) to 7) pressure varies between 0.1 to ca. 70 bar, whereas temperature varies between 20 to ca. 290 °C, respectively. An exception to these is System pressure test, i.e. load transient 1), during which pressure rises to 110 bar, and is kept at that value for a certain number of hours, while temperature stays at 70 °C for the whole duration of the load transient. This load transient is a structural integrity test that is carried out to the primary circuit before start of operation and only once. The most regularly occurring load transients are Cold shut-down and Cold start-up, due to e.g. the yearly outages carried out approximately at the same time each year. During the former load transient pressure and temperature decrease within 6 hours from the above mentioned maximum values to minimum values, corresponding to shut down conditions, whereas in case of the latter load transient, which also lasts 6 hours, the altering of the load parameters is opposite to that, ending to operational conditions. This example also shows how two load transients occurring in consecutive order form a full load cycle. The altering of the load parameters can be also relatively quick in case of some load transients, e.g. during load transients 4), 5) and 7) pressure and temperature change significantly within just tens of seconds. The durations of the load transients 4) to 7) vary approximately between 1 to 31 min (without the static conditions for reaching steady state added before and after). Also other load transients are anticipated to act in the analysed components, however in this study the scope is limited to the above mentioned more relevant and typically occurring load transients.

The above mentioned load transients are taken to form load cycles as follows:

- 1) = LC1,
- 2) & 3) = LC2,
- 4) & 5) = LC3,
- 4) & 6) = LC4,
- 4) & 7) = LC5,

where LC is load cycle and the load transients are assembled in the correct chronological order, i.e. so that the altering of the load parameters begins from and ends to the reference state.

The only considered static system load case is operational conditions, during which pressure stays at 70 bar and temperature in most parts of the primary circuit at 286 °C, respectively. This is also the reference state mentioned above in the connection of the load cycles.

The load effect from the piping system side to the analysed components is such that during operational conditions the tension load, modelled here as axial membrane stress, is ca. 90 MPa, whereas when the plant is shut down, this tension load is zero, and between these two system loading condition extremes it varies linearly.

## WRSs

The stationary welding process induced residual stresses for the analysed safe-end/pipe joint weld are presented in the following. As mentioned earlier, SINTAP procedure [7, 8] is selected for defining the as-welded state WRSs to be used in the FEM simulations in this study.

As for the yield stress of the considered austenitic SSs, the work hardening after the beginning of the plastic deformation must be taken into account as well. In this case, the yield stress  $\sigma_y$  is defined as the 1.0 % proof stress. To a first approximation:  $\sigma_y (\sigma_y = 1.0 \%) \approx 1.5 \cdot \sigma_y (\sigma_y = 0.2 \%)$ , as presented in the SINTAP procedure documentation [7, 8]. The temperature is set to

286 °C in most calculations, corresponding to operational temperature in Finnish BWR NPP units. In this temperature the stress at 0.2 % strain of the considered austenitic weld material is 220 MPa. Here 1.5 times the stress at 0.2 % strain, i.e. 330 MPa, was taken to correspond the stress at 1.0 % strain. The tensile strength of the considered austenitic SS in the mentioned temperature is 586 MPa.

The as-welded state WRSs defined according to SINTAP procedure [7, 8] for the analysed safe-end/pipe joint weld in parallel and perpendicular to weld directions are presented in the following Table 4.1.3-1 and Figure 4.1.3-1. These WRS values are calculated with equations (3.2-1a) to (3.2-1e) and (3.2-2a) to (3.2-2e) here. Though it is not mentioned in the SINTAP documentation [7, 8], it is assumed that these equations define WRSs on the weld centre surface/line.

*Table 4.1.3-1. The as-welded state WRSs defined according SINTAP procedure [7, 8] for the centre surface/line of the analysed safe-end/pipe joint weld of austenitic weld material. Here  $t_{wall}$  is wall thickness at weld location with origin at the inner surface,  $\sigma_R^T$  is transverse to weld WRS component and  $\sigma_R^L$  is longitudinal to weld WRS component.*

| Wall thickness  | Transverse to weld WRSs |                     | Longitudinal to weld WRSs |                     |
|-----------------|-------------------------|---------------------|---------------------------|---------------------|
|                 | $T = 20\text{ °C}$      | $T = 286\text{ °C}$ | $T = 20\text{ °C}$        | $T = 286\text{ °C}$ |
| $t_{wall}$ [mm] | $\sigma_R^T$ [MPa]      | $\sigma_R^T$ [MPa]  | $\sigma_R^L$ [MPa]        | $\sigma_R^L$ [MPa]  |
| 0.0             | 269                     | 245                 | 356                       | 325                 |
| 0.8             | 242                     | 221                 | 357                       | 326                 |
| 1.6             | 215                     | 196                 | 357                       | 326                 |
| 2.4             | 188                     | 172                 | 357                       | 326                 |
| 3.2             | 161                     | 147                 | 357                       | 326                 |
| 4.0             | 134                     | 123                 | 358                       | 326                 |
| 4.8             | 107                     | 98                  | 358                       | 327                 |
| 5.6             | 81                      | 74                  | 358                       | 327                 |
| 6.4             | 54                      | 49                  | 358                       | 327                 |
| 7.2             | 27                      | 25                  | 359                       | 327                 |
| 8.0             | 0                       | 0                   | 359                       | 328                 |
| 8.8             | -27                     | -25                 | 359                       | 328                 |
| 9.6             | -54                     | -49                 | 359                       | 328                 |
| 10.4            | -81                     | -74                 | 360                       | 328                 |
| 11.2            | -107                    | -98                 | 360                       | 329                 |
| 12.0            | -134                    | -123                | 360                       | 329                 |
| 12.8            | -161                    | -147                | 360                       | 329                 |
| 13.6            | -188                    | -172                | 361                       | 329                 |
| 14.4            | -215                    | -196                | 361                       | 330                 |
| 15.2            | -242                    | -221                | 361                       | 330                 |
| 16.0            | -269                    | -245                | 362                       | 330                 |

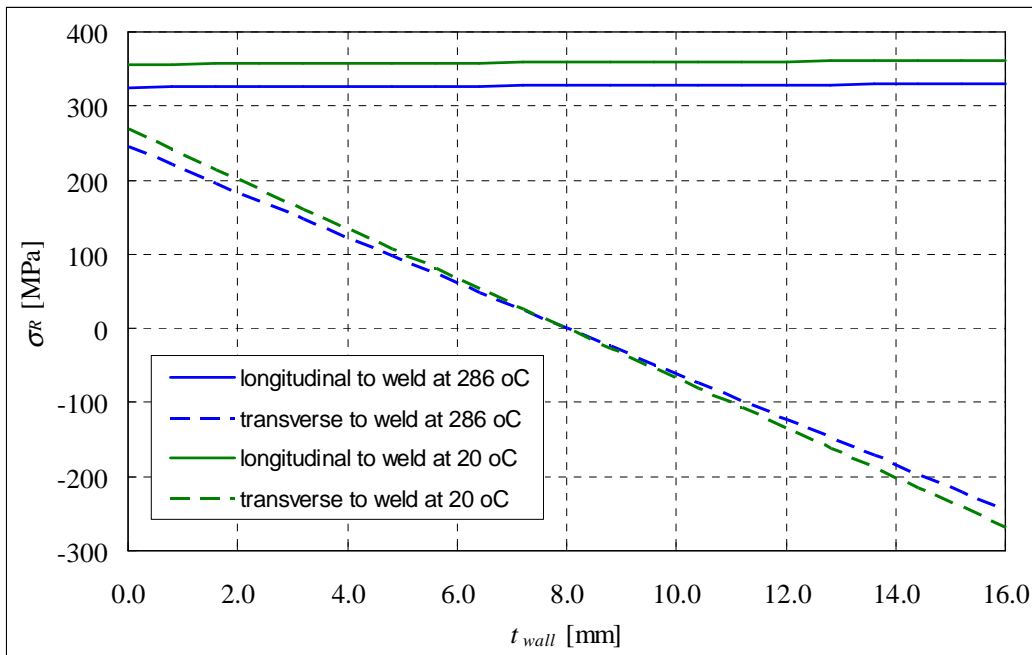


Figure 4.1.3-1. The as-welded state WRSs defined according SINTAP procedure [7, 8] for the centre surface/line of the analysed safe-end/pipe joint weld of austenitic weld material. Here  $t_{wall}$  is wall thickness at weld location with origin at the inner surface, and  $\sigma_R$  is WRSs.

### Load history used in FEM analyses

In order to obtain a realistic load history, one load transient needs to be considered in addition to those mentioned above. Namely, after System pressure test the plant is in the state of shut-down. For the operation of the plant to begin, the pressure and temperature need to be elevated to the values corresponding to the operational conditions. Thus a load transient called here Start of operation (SO), taken as identical to load transient Cold start-up, is added here to occur after System pressure test and ensuing associated steady state (STS). The load sequence applied here as a single load history in the time dependent FEM analyses, and using the notations presented above, is as presented in the following Table 4.1.3-2.

In the FEM analyses the above described temperature and pressure loads were set to the inner surfaces of the analysis model. At all times the pressure of 1.0 bar and temperature of 20 °C, respectively, were set to the outer surfaces of the model. The above depicted WRSs, on their behalf, were assumed to prevail throughout the examined safe-end/pipe joint weld.



Table 4.1.3-2. The load sequence applied here as a single load history in the time dependent FEM analyses. Note that in case of two load transients forming a load cycle there is also a phase of static loading to steady state between the two transients.

|                        |  |                   |   |                   |
|------------------------|--|-------------------|---|-------------------|
| <b>Event no.</b>       | <b>1</b>   | <b>2</b>          | <b>3</b>  | <b>4</b>          |
| <b>Event descript.</b> | STS => WRS => STS  | STS => LC1 => STS | STS => SO => STS  | STS => LC2 => STS |
| <b>Event no.</b>       | <b>5</b>   | <b>6</b>          | <b>7</b>  | <b>8</b>          |
| <b>Event descript.</b> | STS => LC3 => STS  | STS => LC4 => STS | STS => LC2 => STS   | STS => LC5 => STS |
| <b>Event no.</b>       | <b>9</b>   | <b>10</b>         | <b>11</b>   | <b>12</b>         |
| <b>Event descript.</b> | STS => LC2 => STS  | STS => LC3 => STS | STS => LC2 => STS   | STS => LC4 => STS |
| <b>Event no.</b>       | <b>13</b>  | <b>14</b>         | <b>15</b>   | <b>16</b>         |
| <b>Event descript.</b> | STS => LC2 => STS  | STS => LC3 => STS | STS => LC2 => STS   | STS => SDS => STS |
| <b>Notations</b>       | <ul style="list-style-type: none"> <li>• STS; static loading to steady state</li> <li>• WRS; loading of WRSs</li> <li>• SO; Start of operation</li> <li>• SDS; shut-down state (i.e. static pressure of 1.0 bar and temperature of 20 °C, respectively)</li> </ul> |                   | <ul style="list-style-type: none"> <li>• LC1; System pressure test</li> <li>• LC2; Cold shut-down &amp; Cold start-up</li> <li>• LC3; Feed water line opened at 320 kg/s &amp; Reactor scram, during normal operation with normal feed water flow</li> <li>• LC4; Feed water line opened at 320 kg/s &amp; Feed water line closed at 320 kg/s</li> <li>• LC5; Feed water line opened at 320 kg/s &amp; A – isolation</li> </ul> |                   |

## 4.2 Heat transfer and stress/strain analyses

The prepared FEM model is presented in the following, together with the associated boundary conditions. This follows with a presentation of the performed heat transfer and stress/strain FEM simulations.

All heat transfer and stress/strain analyses were performed with FEM code Abaqus, version 6.8-2 [11, 12]. The analyses were performed as fully coupled. This means that the heat transfer and stress/strain analyses were performed simultaneously.

With Abaqus the time incrementation in a transient heat transfer analysis can be controlled directly by the user or automatically by the analysis code. Automatic time incrementation is generally preferred [12]. However, here due to the selected fully coupled analysis type, only user predetermined incrementation is allowed by the analysis code. This is carried out as a function of time, so that for each analysis step (load transient here) a suitable time increment is selected, i.e. these increments are analysis step specific.

A transient analysis with Abaqus can be terminated by completing a specified time period, or it can be continued until steady state conditions are reached, depending on the value of the analysis end parameter [12]. The latter option was used in the analyses here. Steady state is defined by the temperature change rate: when the temperature at every temperature degree of freedom changes at a rate that is less than the specified rate, the analysis terminates [12]. A suitably small value for the temperature change rate was chosen for the analyses, in all cases 1 °C or less.

For all analysed components the stress free temperature in the stress analyses was chosen as 286 °C, for justifications see e.g. reference [15]. In the Abaqus analyses this is included in the analyses in the form of so called reference temperature, which is related to the stress free temperature.

Main results from the heat transfer and stress/strain analyses are presented in Section 4.2.3.

## 4.2.1 FEM model and boundary conditions

As all considered loads, including WRS distributions, are symmetric in relation to geometry symmetry axis of the examined safe-end, pipe and their joint weld, it was sufficient to prepare an axisymmetric FEM model for the needed numerical simulations.

The boundary conditions of the FEM model of the examined safe-end, pipe and their joint weld, used in the fully coupled heat transfer and stress/strain analyses, are described in the following.

### Thermal and displacement boundary conditions

The thermal boundary conditions of the FEM model of the examined safe-end, pipe and their joint weld are the following:

1. The outer surfaces, see Figure 4.1.1-1, are isolated and the heat transfer through the isolation is insignificant as compared to the heat transfer caused by the considered loads. Therefore an adiabatic boundary condition was applied, i.e.  $\alpha_{HT} = 0 \text{ W/m}^2\text{K}$ .
2. At the cut-off sections at the safe-end and pipe ends, see Figure 4.1.1-1, no heat exchange will exist that influence the examined phenomena, i.e. in both surfaces the heat transfers to in and out directions are equal, and thus cancel each other. Therefore an adiabatic boundary condition was applied, i.e.  $\alpha_{HT} = 0 \text{ W/m}^2\text{K}$ .
3. At the inner surfaces, see Figure 4.1.1-1, heat will be exchanged between the water and the metal. The amount of heat that will be exchanged is controlled by the heat transfer coefficient  $\alpha_{HT}$ , and its values vary between 1000 and 70000  $\text{W/m}^2\text{K}$ .

The displacement boundary conditions of the examined safe-end and pipe are the following:

1. At the safe-end side vertical cut-off surface, see Figure 4.1.1-1, the horizontal displacements are set to zero. Thus the model is horizontally fixed in this plane.
2. At the pipe side vertical cut-off surface, see Figure 4.1.1-1, the model is exposed to loads from the piping, which are described in Section 4.1.3. This surface is set to remain vertical and straight, but allowed to deform perpendicular to itself.

### FEM model

The element mesh created for the examined safe-end, pipe and their joint weld is shown in Figures 4.2.1-1 and 4.2.1-2.

In the direction of the model symmetry axis, being y-axis in the two Figures, the length of the FEM model is approximately 750 mm. In general, the geometry of the analysed components and material property data of the associated materials needed to create the FEM model are presented in Sections 4.1.1 and 4.1.2, respectively. The loads acting on the FEM model are presented in Section 4.1.3.

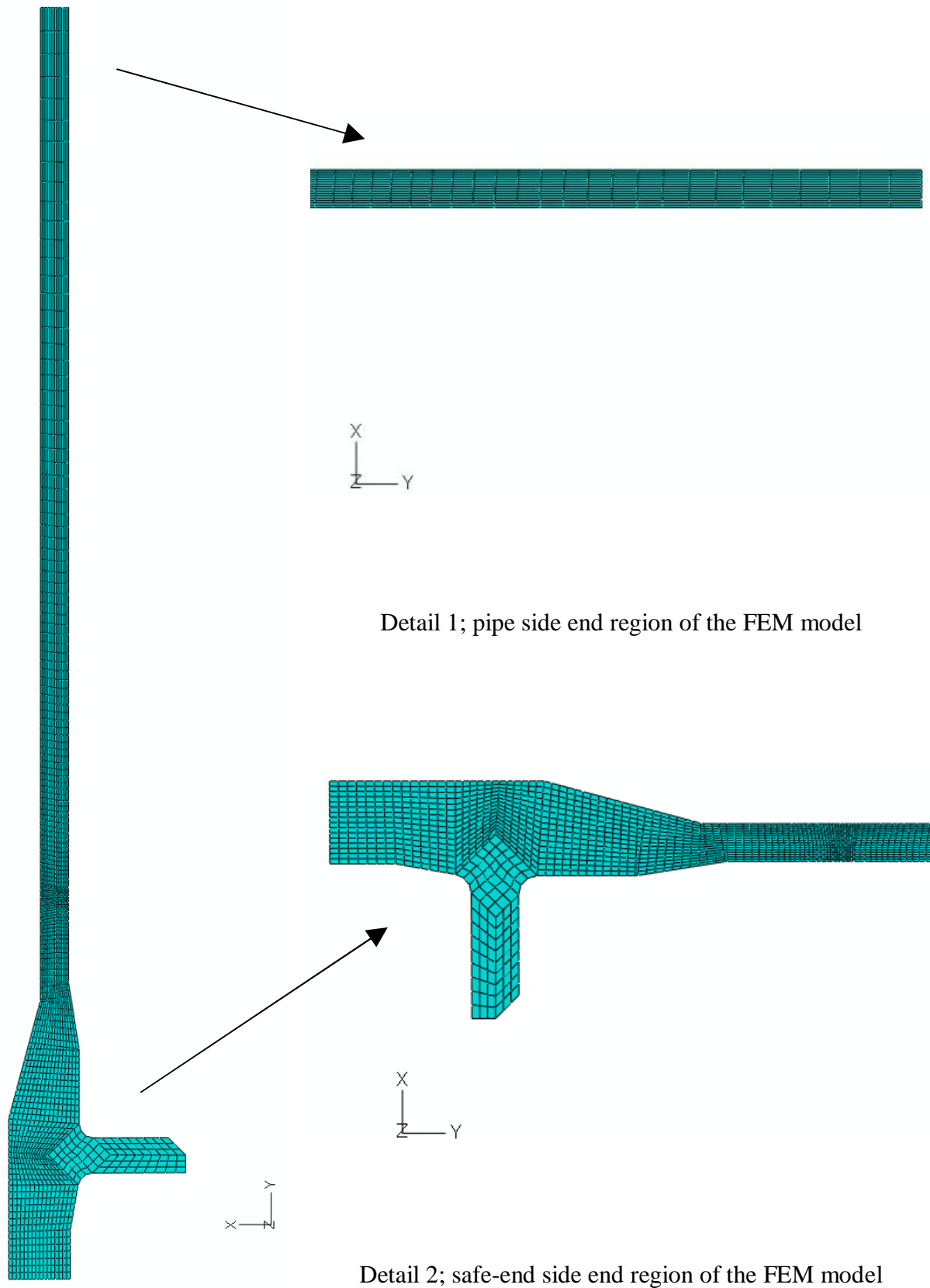
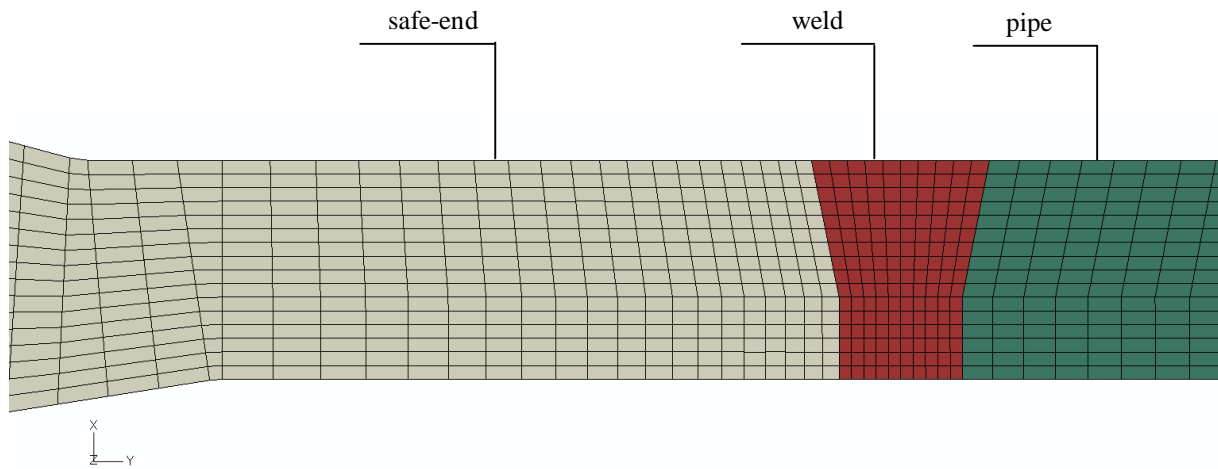


Figure 4.2.1-1. The overall element mesh and two mesh details of the axisymmetric FEM model of the examined safe-end, pipe and their joint weld.



*Figure 4.2.1-2. Detail of the element mesh of the axisymmetric FEM model of the examined safe-end, pipe and their joint weld, showing all involved material regions emphasised with different colours. For the location of this detail in the complete element mesh, see Figure 4.2.1-1.*

As can be seen from Figures 4.2.1-1 and 4.2.1-2, the number of elements over the wall in the model is 16. The side lengths of the elements varied between 1 to 13 mm in the model, with smallest element size and highest density in the region of the examined safe-end/pipe joint weld.

The axisymmetric FEM model was meshed with general purpose continuum elements. The selected element type from the Abaqus element library is CAX4RT, which is a 4-node rectangular bilinear displacement and temperature element, with reduced integration and hourglass control. Active degrees of freedom are the two displacements in the model plane, i.e. in the vertical ( $x$ -axis) and horizontal ( $y$ -axis, being here also the FEM model symmetry axis) directions, and temperature. The number of the nodes and elements in the model are 2836 and 2650, respectively.

## 4.2.2 Aspects concerning modelling of WRSs with FEM

In this study it was attempted create to a simple and robust approach to model WRSs with FEM. Nowadays in advanced FEM analysis codes, such as Abaqus, there are several load types available. Some of those are applicable for creating local initial loads, such as WRSs. A number of drawbacks and challenges as well as possible solutions were encountered and found, respectively, when examining suitable WRS modelling options for practical FEM analysis purposes. A summary of these aspects is presented in the following.

As a starting point, almost any approach to create a locally high stress state matching the selected WRS distribution to a FEM model can be applied, as long as it remains as such when the loading with which it is created is removed. In practise this means that if in the analysis steps following the one during which WRS distribution was created, which obviously should be the very first analysis step, no other loading is introduced to the analysis run, the total stress state in the examined weld region should correspond the WRS distribution. Obviously the total stress state changes in the FEM model weld region, when other loads are introduced

to the model further in the analysis run, and if the yield strength is exceeded WRSs and other stress components may lower to some extent as the stresses further distribute to the neighbourhood of the weld region.

As mentioned earlier, a history of anticipated load transients were analysed. This means that they were all included in a single analysis run in a realistic chronological order and separated from each other by static loading conditions long enough for steady state to take place. Thus the effect of structural memory, i.e. the effect to each present material elastic-plastic stress/strain state of all earlier loads, was fully included. Such FEM analysis runs easily turn out to be computationally very laborious. Thus it is essential to use as small a model as possible so that all necessary and relevant physical phenomena and characteristics remain included in it, in order to minimise the total number of analysis Degrees Of Freedom (DOFs). If it is possible to use an axisymmetric FEM model, as it is in this study, it remarkably lessens the computational burden as compared to the use of a full 3D FEM model. The sizes of the models of the latter type can be prohibitively large, allowing the inclusion of only a few load transients to a single analysis run, when tens of them should be possible to include to it when simulating plant operation spanning only a few years. However, one possibility to come to terms with this drawback at least to some extent would be to use sub-modelling technique. Then the global FEM model could have a relatively coarse element mesh, and only the sub-model within which the examined weld is located would have a dense element mesh. When using this technique it is important that the edges of the sub-model are far enough from the region of interest, e.g. a weld, so that the possible boundary condition disturbances would even out enough well before this region.

When creating a local WRS distribution to a FEM model, it is generally not possible to apply the most commonly used load types, such as pressure, line and point loads against a surface. Thus other load types must be resorted to. The number of available load types depends also on the used FEM analysis code.

Among the most promising load types provided by Abaqus from the viewpoint of modelling WRSs are the Initial Conditions and Body Force. The simulation of WRS distribution in the safe-end/pipe joint weld region in the created axisymmetric analysis model, see Section 4.2.1, was attempted with both of these load types. With Initial Conditions it is possible to set constant value stresses to element edges/faces, whereas with Body Force it is possible to set density forces to act on elements, or more specifically throughout their volumes, as the physical dimension this load type is  $\text{N/m}^3$ . With the latter load type it is also possible to set the loads time dependently, by using a time Amplitude option. With both of these load types it is possible to set loads to inside FEM models.

It was soon noticed that the stiffness of the model, as e.g. dependent on the length of the model in relation to its thickness, and applied boundary conditions strongly affect how the FEM model responds to these locally high loads, i.e. how it further distributes them within the model. Thus the set of load values with which a correct local WRS distribution is achieved is always unique to each FEM model. Here the prepared FEM model was relatively slender, i.e. quite long as compared to its other dimensions, which was to ensure that possible boundary condition disturbances even out well before the examined weld. With the boundary conditions in the used FEM model, i.e. safe-end side edge fixed and pipe side edge limited to remain vertical but allowing horizontal deformation, it was not reasonably, let alone accurately, possible to create the needed WRS distribution, see Table 4.1.3-1 and Figure 4.1.3-1, with Initial Conditions. However, these boundary conditions were maintained in order to be able to set the tension loads from the piping system to the vertical cut-off pipe edge. It is not possible to set any loads to such an edge or surface to which any fixed boundary conditions are

imposed. As fixed boundary conditions were already set to the safe-end side edge of the FEM model, the pipe side edge of the model had to be kept free from those. Besides, it would have violated realism to have fixed boundary conditions at the pipe side edge, as the piping system does not provide a strong barrier against deformations, but responds to deformations relatively flexibly instead. On the other hand, it is realistic to have fixed boundary conditions at the safe-end side vertical cut-off edge, as this component is welded to the nozzle, which is a considerably stiff component and is on its behalf welded to the RPV, which is a very heavy and stiff component, thus providing a considerably strong barrier against deformations from the components attached to it.

With Initial Conditions the local stress field in the safe-end/pipe joint weld region of the FEM model, after continuing the WRS analysis step to steady state, resulted after several attempts with different initial stress values and distribution shapes in all cases in either remarkably too low or too high stress levels, and also with erroneous distribution shape.

With Body Force it was possible to create such a local stress field in the safe-end/pipe joint weld region of the FEM model that after continuing the WRS analysis step to steady state the result was a somewhat correct local WRS distribution, both concerning maximum and minimum values and distribution shape. However, this took several attempts. Also this was possible only in one direction at a time. More precisely, when an approximately correct WRS distribution was achieved at the end of WRS loading analysis step in transverse (i.e. perpendicular to weld) direction, the same was not possible to achieve within the same WRS analysis step in the longitudinal (i.e. parallel to weld) direction, regardless of the several attempts with various stress load values. The same outcome was also met when having obtained approximately correct longitudinal WRSs and attempting to create the corresponding transverse ones. The examined safe-end/pipe joint weld resembles more NPP piping welds than those joining cylinder shaped components with thicker walls. Thus it was decided to limit the examination here to concern only transverse WRSs, as worldwide more than 90 % of the encountered/detected primary circuit piping crack cases have been oriented longitudinally, see e.g. ref. [22], and it is mainly transverse stresses that make such cracks grow.

So, creating local stress fields of WRS type to a FEM model is in practise an iterative process. First an applicable load type must be selected. Then as an initial approximation a set of load values must be selected. Based on the achieved local stress field in the end of WRS analysis step, the load values are to be justified, e.g. providing higher values if the resulting WRS distribution had too low maximum values, and run the analysis step again. This iterative process is continued until a correct enough WRS distribution has been achieved.

Like most of the other more recently published WRS procedures, also SINTAP procedure documentation [7, 8] provides distributions for how the WRSs even out when receding from the weld. This is taken to occur within the length of the calculated radius of the yield zone,  $r_0$  [mm], which is typically of the scale of the associated wall thickness, see Figure 3.2.1. In the FEM analyses the weld centre line WRS distribution was assumed to act in the whole of the weld region, and letting it even out by itself in the adjacent material regions, resulting with reasonably well matching falling WRSs as compared to those according to SINTAP procedure [7, 8].

One option to create local WRS distributions to a FEM model that was due to work schedule limitations not attempted here, is to use such values for the coefficient of thermal expansion in the weld region that the resulting stress field within the covered temperature range in the actual analyses would match the desired WRS distribution. When using this approach the values of the coefficient of thermal expansion for the other material regions would be



maintained in their original (i.e. correct) values, or modified slightly. This approach might be applied in the next phase of this project.

### 4.2.3 Summary of FEM analysis results

In the following is a presentation concerning the heat transfer and stress/strain analysis results. As mentioned earlier, the analyses were performed with FEM code Abaqus, Version 6.8-2 [11, 12] as fully coupled thermal-stress/strain analyses. Due to the large amount of analysis result data, only a summary of them is presented here. It was decided to limit the presentation here to concern only transverse WRSs, as worldwide more than 90 % of the encountered/detected primary circuit piping crack cases have been oriented longitudinally, see e.g. ref. [22], and it is mainly transverse stresses that make such cracks grow.

As the location of most interest is the safe-end/pipe joint weld, the result presentation here is mainly focused on that region. The analyse load cycles and transients, as taken from Section 4.1.3 but not repeating here the static conditions for achieving steady state before and after each load transient, are in the chronological analysis order as follows:

- Event no. 1; Loading of WRSs
- Event no. 2; System pressure test
- Event no. 3; Start of operation
- Event no. 4; Cold shut-down & Cold start-up
- Event no. 5; Feed water line opened at 320 kg/s & Reactor scram, during normal operation with normal feed water flow
- Event no. 6; Feed water line opened at 320 kg/s & Feed water line closed at 320 kg/s
- Event no. 7; Cold shut-down & Cold start-up
- Event no. 8; Feed water line opened at 320 kg/s & A – isolation
- Event no. 9; Cold shut-down & Cold start-up
- Event no. 10; Feed water line opened at 320 kg/s & Reactor scram, during normal operation with normal feed water flow
- Event no. 11; Cold shut-down & Cold start-up
- Event no. 12; Feed water line opened at 320 kg/s & Feed water line closed at 320 kg/s
- Event no. 13; Cold shut-down & Cold start-up
- Event no. 14; Feed water line opened at 320 kg/s & Reactor scram, during normal operation with normal feed water flow
- Event no. 15; Cold shut-down & Cold start-up
- Event no. 16; Shut-down state

For four of these load events the transverse to weld stress results are presented for the safe-end/pipe joint weld centre line as diagrams in Figure 4.2.3-1, and for the weld and to some extent the adjacent material regions as colour surfaces in Figures 4.2.3-2 to 4.2.3-5.

In the Figures 4.2.3-1 to 4.2.3-5 presenting the FEM analysis results the examined time instant concerning each load event is that when the steady state after the ending of load event has been reached. Concerning the stress result diagrams in Figure 4.2.3-1 the values have been taken from the FEM model nodes. In the colour surface result Figures 4.2.3-2 to 4.2.3-5 S22 corresponds to the transverse to weld stresses in units of MPa. For better comparison of WRS results the effect of loads from the piping system have been removed from the presented FEM results in the Figure 4.2.3-1.



The von Mises material yield model with associated flow rule and isotropic work hardening were used in the performed FEM analyses.

As can be seen from the Figure 4.2.3-1, after 15 load events the transverse to weld WRSs in the centre line of the examined weld have decreased in and near the inner and outer surface approximately 50 MPa. Within the wall the WRSs levels have on the other hand to some extent climbed higher, somewhat suggesting that the continuing distribution of the maximum WRSs to the adjacent material regions occurs also in the through weld wall thickness direction. The relaxing of the WRSs was on the weld edges approximately of the same scale as on the centre line.

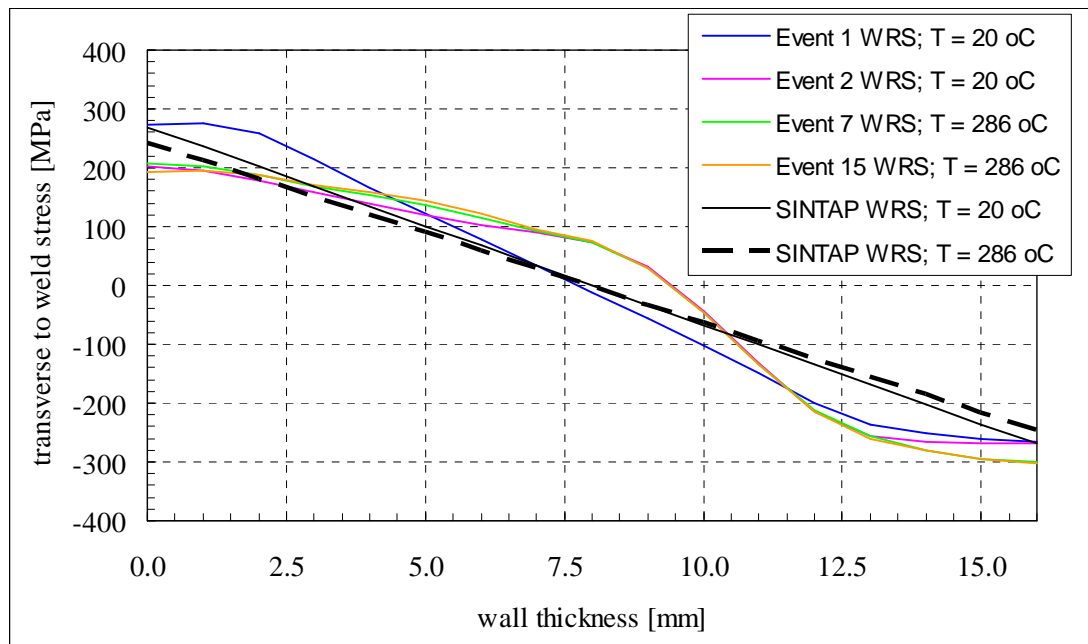


Figure 4.2.3-1. Transverse to weld WRS results for the safe-end/pipe joint weld centre line, together with the corresponding WRS distributions in the as-welded state defined according SINTAP procedure [7, 8]. The examined time instant concerning each load event is that when the steady state after the ending of the load event has been reached. The origin of the radial through wall coordinate axis, horizontal axis in the figure, is at the inner weld surface.

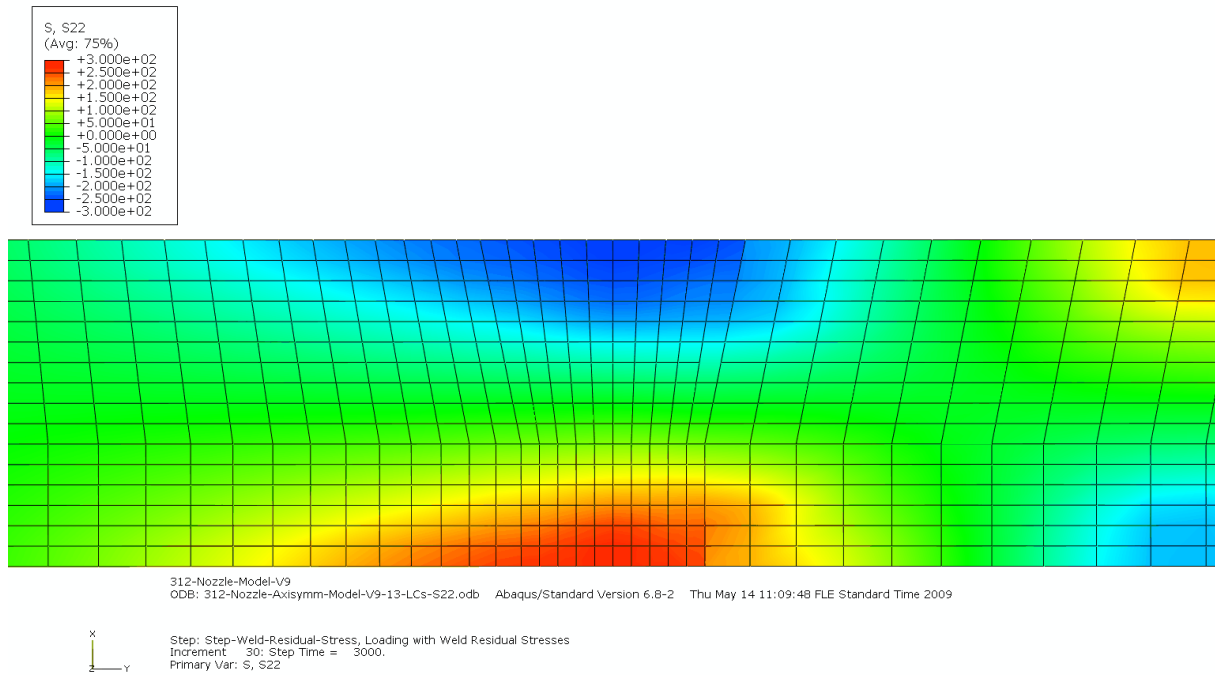


Figure 4.2.3-2. Transverse to weld stress results for the safe-end/pipe joint weld and adjacent regions, here the effects of all associated loads are taken into account. The examined time instant is the steady state after the ending of the load event 1. Here the unit of  $S_{22}$  in the legend is MPa. The prevailing temperature is 20 °C.

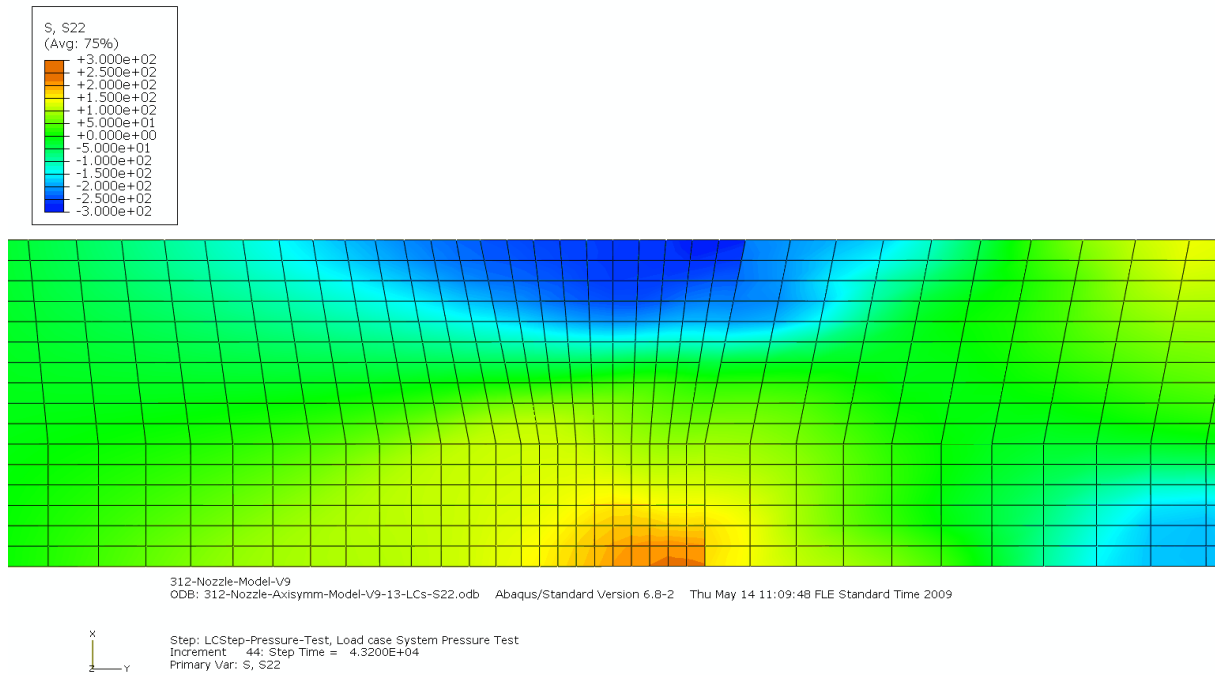


Figure 4.2.3-3. Transverse to weld stress results for the safe-end/pipe joint weld and adjacent regions, here the effects of all associated loads are taken into account. The examined time instant is the steady state after the ending of the load event 2. Here the unit of  $S_{22}$  in the legend is MPa. The prevailing temperature is 20 °C.

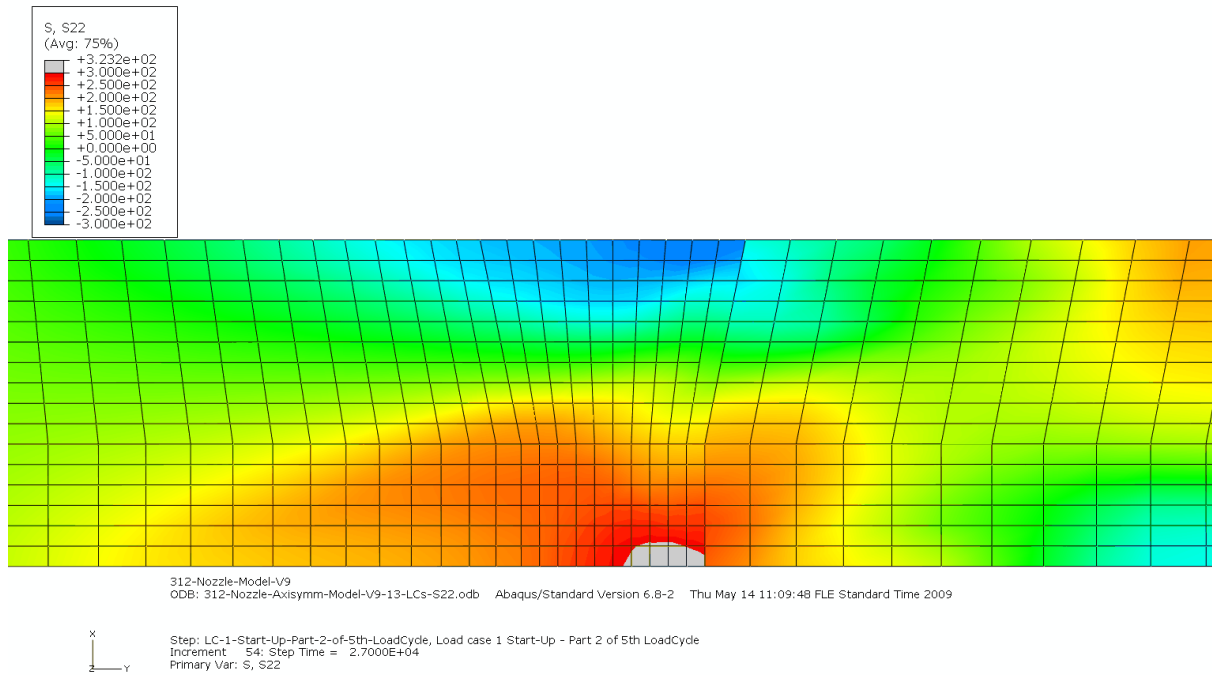


Figure 4.2.3-4. Transverse to weld stress results for the safe-end/pipe joint weld and adjacent regions, here the effects of all associated loads are taken into account. The examined time instant is the steady state after the ending of the load event 7. Here the unit of S22 in the legend is MPa. The prevailing temperature is 286 °C.

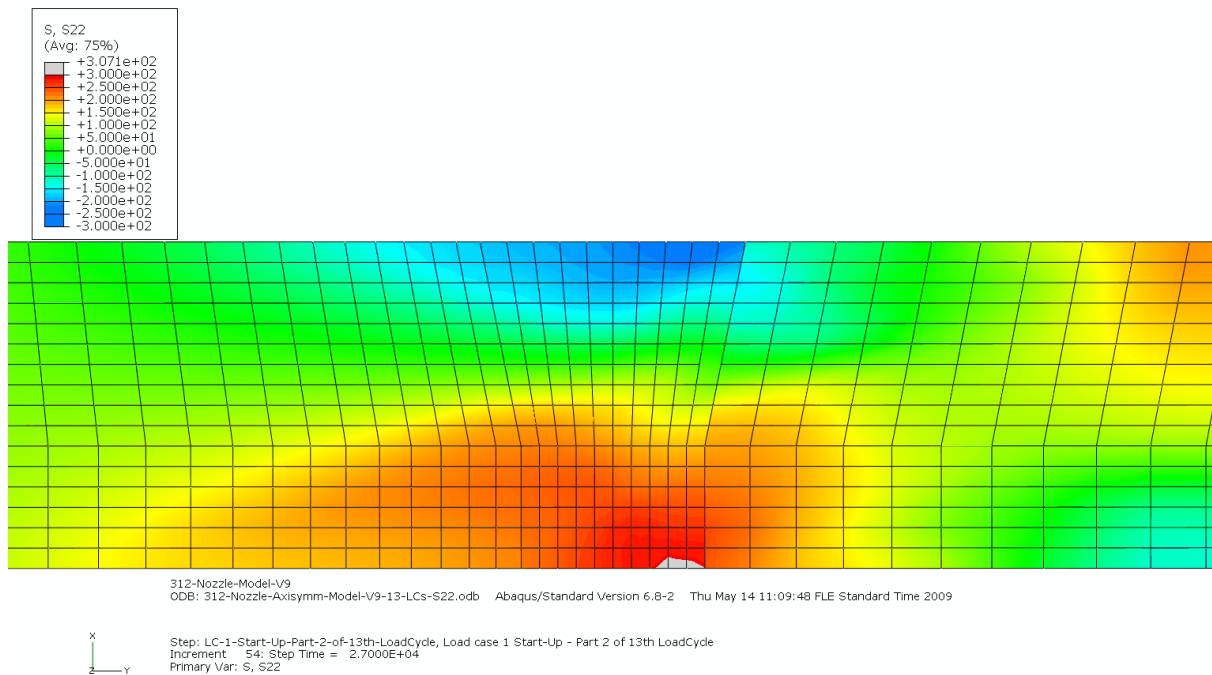


Figure 4.2.3-5. Transverse to weld stress results for the safe-end/pipe joint weld and adjacent regions, here the effects of all associated loads are taken into account. The examined time instant is the steady state after the ending of the load event 15. Here the unit of S22 in the legend is MPa. The prevailing temperature is 286 °C.

Here the von Mises material yield model was used in the FEM simulations, as it is often applied for metals in elastic-plastic analyses, and it is also computationally relatively easy to use. Likewise it is appropriate to use associated flow rule in this connection. However, isotropic work hardening is not necessarily the most appropriate model to depict the elastic-plastic behaviour history of the ductile austenitic SS weld material here. Instead, kinematic or combined isotropic and kinematic work hardening model could better and more realistically suit for the analysis task in question. However, due to lack of available material data during the preparation of the FEM analyses, it was not possible to apply either of these two mentioned work hardening modelling options.

Another inevitable departure from realism in the FEM analyses concerns the modelling of the material properties in the Heat Affected Zones (HAZs) adjacent to the weld question. Namely, in HAZ regions the material properties somewhat continuously change from those corresponding to the weld material to those corresponding to the adjacent base materials. However, again due to lack of material data it was not possible to include these characteristics in the numerical simulations.

The use of an axisymmetric model and to a somewhat optimised element mesh resulted with computationally very economical FEM analyses. With a 2.0 GHz PC having two CPUs and 2.0 GB of RAM memory the final FEM analysis run comprising altogether 28 consecutive load transients took only slightly less than two hours to complete. Thus it can be concluded that with the present day efficient PCs it is computationally feasible to perform time dependent thermal-stress/strain FEM analyses covering considerably lengthy load sequences comprising tens of individual load transients, when suitably optimised analysis models are used.

## 5 Fracture mechanics based crack growth analyses including WRS distributions

The fracture mechanics based crack growth analyses including WRS distributions are presented in this chapter. The scope is limited to two cases: a crack growth analysis considering the WRS component of the stresses acting in the examined weld to remain at as-welded state as defined according to the SINTAP procedure [7, 8], and a crack growth analysis with all stresses taken from the results of the FEM analyses, of which a summary is presented in Section 4.2.3. However, when considering a realistic duration of plant operation within which the load events analysed here with FEM would occur, they are assumed to span approximately only one year. The planned operational lifetimes of NPPs are on the other hand much longer than that, e.g. 60 years. This matter does not concern the first of the mentioned two crack growth analyses, as in that case all stress components are taken to remain as such, i.e. they are time independent. However, in case of the second of the mentioned two crack growth analyses it was assumed that the stress distributions within the weld region remain as they are after the last analysed load event for the rest of the assumed operational plant lifetime. Here the assumed operational plant lifetime is 60 years. The degradation mechanism and load case considered in the crack growth analyses are intergranular stress corrosion cracking (IGSCC) and static operational conditions, respectively.

The structure of this chapter is such that the crack growth analysis input data, procedure and tool are presented first, and after that a summary of the analysis results.

### 5.1 Crack growth analysis input data, analysis procedure and analysis tool

#### Input data to fracture mechanics based analyses

The dimensions and material properties of the analysed safe-end/pipe joint weld are presented in Sections 4.1.1 and 4.1.2, respectively. The process loads considered here are those corresponding to static operational conditions, i.e. pressure of 70 bar and temperature of 286 °C, respectively, see Section 4.1.3. The analysed degradation mechanism is IGSCC.

The experimentally defined parameter values used in the crack growth equation for IGSCC and which characterise the material properties as a function of temperature and environment are presented in Table 5.1-1.

*Table 5.1-1. Values of parameters  $C$  and  $n$  used in the IGSCC equation, equation (5.1-1) in the following, for considered austenitic SS weld material. The dimensions used in the crack growth equation are:  $[da/dt] = \text{mm/year}$ , in which  $K_I [\text{MPa}\cdot\sqrt{\text{m}}]$  is mode I stress intensity factor (SIF-I),  $a [\text{mm}]$  is crack depth, and  $t [\text{year}]$  is time, see ref. [23].*

| $C$                   | $n$  | Environment |
|-----------------------|------|-------------|
| $1.42 \cdot 10^{-04}$ | 3.00 | water       |

For the examined safe-end/pipe joint weld two crack growth analysis cases are considered:

1. The WRS component of the stresses acting in the weld remaining at as-welded state as defined according to the SINTAP procedure [7, 8], and with stresses caused by process loads as taken from Section 4.1.3, respectively. In this case all stress components are set to remain as such, i.e. they are time independent. Here the WRSs were added to other stress components by superposition to obtain the total stress distribution.
2. The WRS component and other stresses are taken time dependently from the results of the performed FEM analyses, of which a summary is presented in Section 4.2.3. In this case it was assumed that the stress distributions within the weld region remain as they are after the last analysed load event.

In both crack growth analyses the considered crack postulate is a circumferentially oriented inner semi-elliptic surface crack, with aspect ratio, i.e. crack depth divided by half of crack length, set to a constant value of 1/3. This is equal to the aspect ratio of the reference crack as defined in Section III of the ASME code [24], corresponding to the crack shape having the highest growing potential. The dimensions of the initial crack postulate are: depth x length = 0.1 x 0.6 mm. The analyses cover an assumed operational plant lifetime of 60 years. As for the considered crack postulate the opening mode (mode I) is assumed in the analyses, for which the stresses driving the crack growth are taken in the transverse to weld direction. The effect of load transients to IGSCC is omitted, as concerning loads only static operational conditions and WRSs need to be considered in the analyses. It is assumed that the yearly time spent under operational conditions is altogether 8000 h.

The transverse to weld stresses caused by loads from the piping system side is such that during operational conditions the tension load, modelled as axial membrane stress, is ca. 90 MPa, as mentioned in Section 4.1.3.

### Fracture mechanics analysis procedure

SCC is a localised non-ductile progressive failure mechanism that occurs only in case the following three conditions are fulfilled simultaneously, see ref. [25]:

- Stress around the crack-tip is tensile.
- Environment is aggressive.
- Material is susceptible to SCC.

When these conditions are met, the intergranular SCC failure mode, IGSCC, is considered in the associated analyses.

SCC is a delayed failure process. That is, cracks initiate and propagate at a slow rate until the stresses in the remaining ligament of metal exceed the fracture strength. The sequence of events involved in the SCC process is, according to ref. [26], usually divided into three stages:

1. Crack initiation.
2. Steady state crack propagation.
3. Final failure.

The fracture mechanics based crack growth equation used in the analyses, which depicts the intermediate (stage 2) SCC, is according to reference [27]:

$$\frac{da}{dt} = C \cdot K_I^n \quad (5.1-1)$$

where  $C$  and  $n$  are constants characterising the material properties as a function of temperature and environment, and the values of which were given in Table 5.1-1. Also the other variables/parameters of this equation have been presented earlier. No  $K_I$  threshold value was considered in the IGSCC induced crack growth analyses.

In all analyses, the  $K_I$  values were calculated with analysis tool VTTBESIT, the characteristics of which are briefly described in the following.

### **Fracture mechanics based analysis tool**

The fracture mechanics based more robust crack growth analyses were performed with the analysis code VTTBESIT. This analysis code comprises parts developed by the Fraunhofer-Institut für Werkstoffmechanik (IWM), Germany and by VTT. The theoretical background and analysis procedures of VTTBESIT are presented in refs. [28, 29, 30].

With VTTBESIT it is possible to calculate stress intensity factor values in several points along the crack postulate fronts, including deepest point (crack tip) and edge/end points. The analysis code treats only the mode I loading in which the direction of the loading is perpendicular to the crack surface (crack opening mode), and the analysis procedure is linear-elastic. These calculations are carried out with program BESIT60, developed by IWM. This program is based on the weight/influence function method. Solutions are provided for "infinite" and semi-elliptical surface crack postulates in straight plates and cylinders.

VTTBESIT uses the BESIT60 program code as a pure stress intensity factor value computing subroutine and applies the results as starting values for crack growth assessments. Two crack growth models are provided in the analysis code: Paris-Erdogan equation for fatigue induced crack growth, and rate equation for SCC, here equation (5.1-1), see ref. [31].

## **5.2 Crack growth analysis results**

The results from the two fracture mechanics based crack growth analyses performed to the examined safe-end/pipe joint weld are presented and discussed in this section.

Figure 5.2-1 shows the crack growth results for the two analysed cases as a function of plant years in operation. As can be seen from the figure, the calculated crack growth is in both cases relatively quick, once the crack depth has exceeded approximately 1.5 mm. Concerning the resulting  $K_I$  distributions over the crack fronts, their maximum values stayed in both analysis cases below  $50 \text{ MPa}\sqrt{\text{m}}$ . In the second analysis case where the relaxing of maximum values WRSs and other stress components had been taken into account with FEM simulations, the calculated crack growth was to some extent slower than in the first case where the as-welded state WRSs and other stress components were maintained in their original values time independently throughout the analysed time span. For instance, in the second case the crack grows to 50 % and 90 % depths of wall thickness in 8.2 and 10.6 years, whereas the same results are for the first case 7.7 and 9.9 years, respectively. On the other hand, concerning the crack growth results for the last 10 % of wall thickness, one should view them with some caution as the accuracy of the results is not as good in the remaining 10 % ligament of the wall as in other wall depths. The slowing down of the crack growth rate (CGR) in both analysed cases when approaching the outer wall surface is caused by the compressive WRS values in that part of the wall, the compression reaching the maximum value in the outer surface.



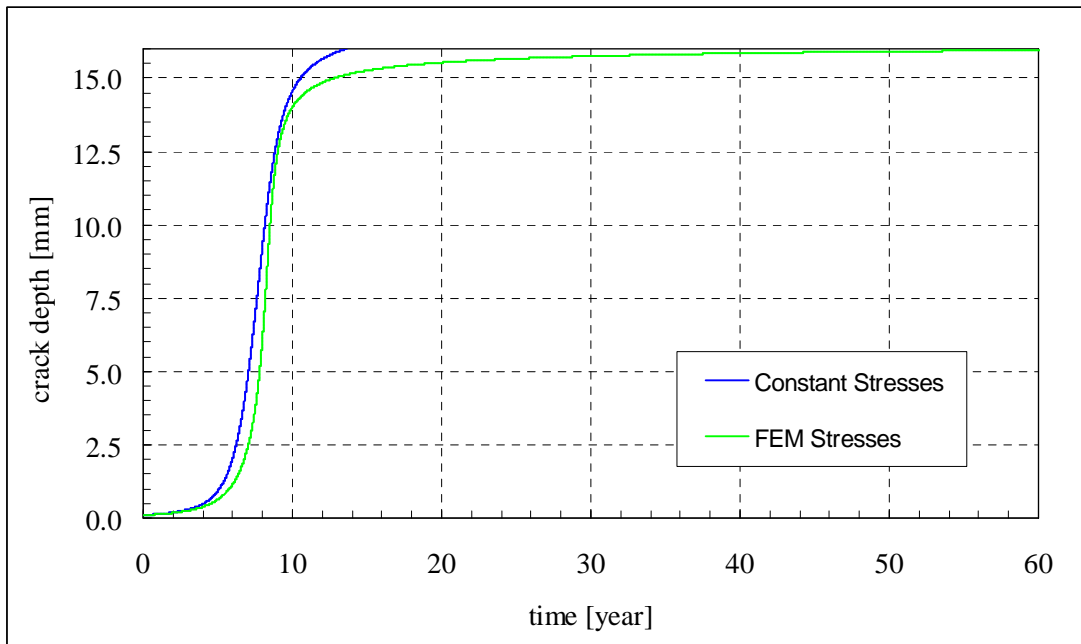


Figure 5.2-1. For semi-elliptic inner circumferential surface crack postulate under axial stresses, including the as-welded WRSs according to SINTAP procedure [7, 8], the crack growth histories through the safe-end/pipe joint weld for two IGSCC analysis cases: 1) stresses remain as they are at the start of analysis (Constant Stresses in the legend), and 2) stresses are taken from the results of the time dependent FEM analyses (FEM Stresses in the legend).

One feature increasing the CGR in the calculations is the applicable but somewhat conservative CGR equation used here, see equation (5.1-1). Namely, the values for the temperature and environment dependent parameters  $C$  and  $n$ , see Table 5.1-1, in this equation have been defined so that the resulting CGR curve envelops almost all associated laboratory data points, i.e. an upper bound approach. The conservative nature is moreover even emphasised in this approach, as the vertical axis presenting the CGR is typically logarithmic, i.e. a seemingly small rise of the CGR curve in the diagram leads to a considerable increase in the corresponding growth rate. All other available applicable CGR procedures for SCC in NPP components in BWR environment appear to be based on the same approach as the one used here, i.e. their temperature and environment dependent parameters have been defined so as to obtain an upper bound CGR curve, see procedures e.g. in refs. [32, 33]. Also, these CGR approaches mostly concern sensitised component materials, whereas presently in many/most NPP units in operation the primary circuit components have been replaced with ones of such materials that are not prone to become sensitised.

One possible way to relieve the conservatism in these CGR assessment procedures would be to apply best estimate approach, i.e. so that the CGR curves would rather be formed as to correspond to the mean values of the underlying laboratory data, than as the mentioned upper bound. This would require access to the underlying measurement data, however, which invariably are proprietary and not available, as CGR tests are expensive to perform, among other things because the test durations are typically of the scale of years. However, for the time being it seems that such best estimate approach, or optionally a probabilistic one, would be the best (and perhaps only) ways to relieve the conservatism in the mentioned CGR procedures. Hopefully this would be possible in the future, which obviously requires first



gaining access to the mentioned CGR laboratory data sources. Having less conservative CGR procedures available would arguably lead to more realistic structural integrity and fitness-for-service analysis results. However, in these analysis procedures at least a reasonable level of conservative approach should be maintained at all times, so as to ensure a sufficient and adequate structural margin against e.g. weaker than designed materials, more severe than anticipated loads and longer than originally designed operational lifetimes.

## 6 Summary, conclusions and suggestions for further research

### Summary and conclusions

This study concerns the welding process induced residual stresses in NPP reactor circuit component welds, and their practical inclusion in structural integrity analyses. The applicability of several commonly used WRS procedures for both FEM simulations and fracture mechanics based crack growth analyses of NPP reactor circuit component welds is assessed and discussed.

According to experimental measurements and FEM analysis results the WRSs are typically relatively high in NPP component welds which are in as-welded state. Thus it is of considerable importance to take them into account in the structural integrity analyses, e.g. cracking sensitivity analyses. The residual stress distributions present in a structure are the result of the manufacturing history and the elastic-plastic properties of the structure. The former referring to the mechanical and thermal processes executed during the whole production sequence and the latter to the elastic-plastic behaviour of the structure. After PWHT and to some extent after weld repair the WRSs are remarkably lower.

The goal of the work here is to study via numerical simulations how the WRSs alter over the years in plant operation in primary circuit component welds (e.g. to see if and how much they decrease), due to various typical/expected transient load cases. When having such stress results, it is then examined what is their impact to the corresponding simulated crack growth rates. In the latter analyses a fracture mechanics based analysis tool is used. Especially when a NPP has been in operation for some decades, it could be assumed that the WRSs have relieved at least to some extent due to typical anticipated and repeated mechanical loads. On the other hand, the operational temperature of BWR units is not high enough for considerable time dependent stress relieving caused by creep to take place.

When looking for a suitable applicable WRS procedure to use in the numerical WRS simulations, the following fitness-for-service procedures were considered: the ASME recommendations [2, 3], the British Standard BS 7910: 1999 [4], the R6 Method, Revision 4 [5], the SAQ handbook [6], the SINTAP Procedure [7, 8], the API 579 procedure [9] and the FITNET Procedure [10]. The selected WRS type here is as-welded state. The WRS definitions included in the mentioned procedures are based both on the available experimental data and FEM analysis results. The published experimental WRS data have a substantial scatter. Consequently the defined WRS distributions have been developed as tensile upper bound solutions based on the data. However, according to [18, 19, 20, 21], this approach not only lacks consistency for the same type of joints and welding parameters, but can either significantly overestimate the WRS level in some cases, or underestimate it in others.

One unfortunate departure from realism in case of some of the more recent WRS procedures, e.g. R6 Method Rev. 4 and FITNET, is that in the transverse to weld direction the WRSs are mostly not self-balancing. While making local crack growth calculations with a fracture mechanics based analysis tool this feature may not pose remarkable problems, but in case of corresponding 2D or 3D FEM analyses it is quite the other way around, as in order to achieve equilibrium FEM automatically modifies the WRSs towards self-balanced distributions over the component model walls, and thus the original WRS distributions are not maintained.

In the light of the WRS analysis results presented in ref. [13], by the author of this report, only ASME recommendations [2, 3] and SINTAP procedure [7, 8] in all cases, and SAQ handbook in most cases [6], give as-welded state WRS distributions that are self-balancing in the transverse to weld direction. Of them the least over conservative WRS procedure appears to be SINTAP, which was also selected to be used for defining the as-welded state WRSs to be used in the FEM simulations in this study.

The type of the selected component assembly to the FEM analyses is a safe-end joined with welds to a nozzle and pipe, resembling those that connect the feed water system to the RPV in BWR units. The wall thickness in the region of the examined safe-end/pipe joint weld is 16 mm. In particular, it is examined how to simulate with FEM the WRS distributions in the examined weld. The as-welded state WRSs defined according to SINTAP procedure [7, 8] for the analysed weld in perpendicular to weld direction vary linearly from 245 MPa in the inner surface to -245 MPa in the outer surface, for temperature of 20 °C, and from 269 MPa in the inner surface to -269 MPa in the outer surface, for temperature of 286 °C, respectively.

A history of anticipated load transients was analysed with advanced FEM code Abaqus, version 6.8-2 [11, 12]. This means that they were all included in a single analysis run in a realistic chronological order and separated by static loading conditions long enough for steady state to take place. Thus the effect of structural memory, i.e. the effect to each present elastic-plastic stress/strain state of all earlier loads, was fully included. All in all there were 28 analysed load transients of which 16 load events were assembled, most of them being full load cycles. The only considered static load case is operational conditions, during which pressure stays at 70 bar and temperature in most parts of the primary circuit at 286 °C, respectively. This is also the reference state in the connection of the mentioned load cycles.

The heat transfer and stress/strain FEM analyses were performed as fully coupled. This means that the heat transfer and stress/strain analyses were performed simultaneously. As all considered loads, including WRS distributions, are axially symmetric in relation to geometric symmetry axis of the examined safe-end and pipe, it was sufficient to prepare an axisymmetric FEM model for the needed numerical simulations. The boundary conditions used in the FEM model were: safe-end side edge fixed and pipe side edge limited to remain vertical but allowing horizontal deformation,

In this study it was attempted to create a simple and robust approach to model WRSs with FEM. Nowadays in advanced FEM analysis codes, such as Abaqus, there are several load types available. Some of those are applicable for creating local initial loads, such as WRSs.

As mentioned earlier, a history of anticipated load transients were analysed. With FEM such analysis runs easily turn out to be computationally very laborious. Thus it is essential to use as small a model as possible so that all necessary and relevant physical phenomena and characteristics remain included in it, i.e. to minimise the total number of analysis DOFs. If it is possible to use an axisymmetric FEM model, as it is in this study, it remarkably lessens the computational burden as compared to the use of a full 3D FEM model. The sizes of the models of the latter type can be prohibitively large, allowing the inclusion of only a few load transients to a single analysis run, when tens of them should be possible to include to it when simulating plant operation spanning only a few years. However, one possibility to come to terms with this drawback at least to some extent would be to use sub-modelling technique, so that the more densely meshed sub-model would include the examined weld.

When creating local WRS distribution to a FEM model, it is generally not possible to apply the most commonly used load types, such as pressure and point loads against a surface. Thus other load types must be resorted to. The number of available load types depends also on the used FEM analysis code.

Of the load types provided by Abaqus, the Body Force was selected for modelling WRSs in the safe-end/pipe joint weld region in the created axisymmetric analysis model. With this load type it is possible to set density forces to act on elements, or more specifically throughout their volumes, as the physical dimension this load type is  $\text{N/m}^3$ .

It was soon noticed that the stiffness of the model, as e.g. dependent on the length of the model in relation to its thickness/width, and applied boundary conditions strongly affect how the FEM model responds to these loads, i.e. how it further distributes them within the model. Thus the set of load values with which a correct local WRS distribution is achieved, is always unique to the FEM model. Here the prepared FEM model was relatively slender, i.e. quite long as compared to its other dimensions, which was to ensure that possible boundary condition disturbances even out well before the examined weld.

With Body Force it was possible to create such a local stress field in the safe-end/pipe joint weld region of the FEM model that after continuing the WRS analysis step to steady state the result was a somewhat correct local WRS distribution, both concerning maximum and minimum values and distribution shape. However, this took several attempts. Also this was possible only in one direction at a time. More precisely, when an approximately correct WRS distribution was achieved at the end of WRS loading analysis step in transverse (i.e. perpendicular to weld) direction, the same was not possible to achieve within the same WRS analysis step in the longitudinal (i.e. parallel to weld) direction, regardless of the several attempts with various stress load values. The same outcome was also met when having obtained approximately correct longitudinal WRSs and attempting to create the corresponding transverse ones. The examined safe-end/pipe joint weld resembles more NPP piping welds than those joining cylinder shaped components with thicker walls. Thus it was decided to limit the examination here to concern only transverse WRSs, as worldwide more than 90 % of the encountered/detected primary circuit piping crack cases have been oriented longitudinally, see e.g. ref. [22], and it is mainly transverse stresses that make such cracks grow.

So, creating local stress fields of WRS type to a FEM model is in practise an iterative process. First an applicable load type must be selected. Then as an initial approximation a set of load values must be selected. Based on the achieved local stress field in the end of WRS analysis step, the load values are to be justified, e.g. providing higher values if the resulting WRS distribution had too low maximum values. This iterative process is continued until a correct enough WRS distribution has been achieved.

According to FEM results, after the analysed load events the transverse to weld WRSs in the centre line of the examined weld have decreased in and near the inner and outer surface approximately 50 MPa. Within the wall the WRSs levels on the other hand climbed to some extent higher, somewhat suggesting that the continuing distribution of the maximum WRSs to the adjacent material regions occurs also in the through weld wall thickness direction. The relaxing of the WRSs was on the weld edges approximately of the same scale as on the centre line.

Here the von Mises material yield model was used in the FEM simulations, as it is often applied for metals in elastic-plastic analyses, and it is also computationally relatively easy to use. Likewise it is appropriate to use associated flow rule in this connection. However,

isotropic work hardening, which was used here, is not necessarily the most appropriate model to depict the elastic-plastic behaviour history of the ductile austenitic SS weld material in question here. Instead, kinematic or combined isotropic and kinematic work hardening model could better and more realistically suit for the analysis task in question. However, due to lack of available material data during the preparation of the FEM analyses, it was not possible to apply either of these two mentioned work hardening modelling options.

Another inevitable departure from realism in the FEM analyses concerns the modelling of the material properties in the HAZs adjacent to the weld question. Namely, in HAZ regions the material properties quite continuously change from those corresponding to the weld material to those corresponding to the adjacent base material. However, due to lack of material data it was not possible to include these characteristics in the numerical simulations.

The use of an axisymmetric model and to some extent optimised element mesh resulted with computationally very economical FEM analyses. With a 2.0 GHz PC having two CPUs and 2.0 GB of RAM memory the final FEM analysis run comprising altogether 28 consecutive load transients took only slightly less than two hours to complete. Thus it can be concluded that with the present day efficient PCs it is computationally feasible to perform time dependent thermal-stress/strain FEM analyses covering considerably lengthy load sequences comprising tens of individual load transients, when suitably optimised analysis models are used.

For the safe-end/pipe joint weld two crack growth analysis cases were considered:

1. The WRS component of the stresses acting in the examined weld remaining at as-welded state as defined according to the SINTAP procedure [7, 8], and with other stresses as caused by process loads. In this case all stress components are set to remain as such, i.e. they are time independent. Here the WRSs were added to other stress components by superposition to obtain the total stress distribution.
2. The WRS component and other stresses taken from the results of the performed FEM analyses. In this case it was assumed that the stress distributions within the weld region remain as they are after the last analysed load event.

In both crack growth analyses, performed with a fracture mechanics based analysis tool, the considered crack postulate is a circumferentially oriented inner semi-elliptic surface crack, with aspect ratio, i.e. crack depth divided by half of crack length, set to a constant value of 1/3. This is equal to the aspect ratio of the reference crack as defined in Section III of ASME code [24], corresponding to the crack shape having the highest growing potential. The dimensions of the initial crack postulate are: depth x length = 0.1 x 0.6 mm. The analyses cover an assumed operational plant lifetime of 60 years. As for the considered crack postulate the opening mode (mode I) is assumed in the analyses, for which the stresses driving the crack growth are taken in the transverse to weld direction. In the crack growth analyses the considered degradation mechanism and load case were IGSCC and static operational conditions, respectively.

In the fracture mechanics based CGR analyses the commonly applied rate equation was used, which depicts intermediate (stage 2) SCC. It includes parameters  $C$  and  $n$  which characterise the material properties as a function of temperature and environment. Analysis tool VTTBESIT, which has been partly developed at VTT, was used in the CGR analyses.

The calculated crack growth was in both analysis cases relatively quick, once the crack depth had exceeded approximately 1.5 mm. In the second analysis case where the relaxing of maximum values WRSs and other stress components had been taken into account with FEM

simulations, the calculated CGR was to some extent slower than in the first case where the as-welded state WRSs and other stress components were maintained in their original values time independently throughout the analysed time span. For instance, in the second case the crack grows to 50 % and 90 % depths of wall thickness in 8.2 and 10.6 years, whereas the corresponding results are for the first case 7.7 and 9.9 years, respectively. The slowing down of the CGR in both analysed cases when approaching the outer wall surface is caused by the compressive WRS values in that part of the wall, the compression reaching the maximum value in the outer surface.

One feature increasing the CGR in the calculations is the applicable but somewhat conservative CGR equation used here. Namely, the values for the temperature and environment dependent parameters  $C$  and  $n$  in this equation have been defined so that the resulting CGR curve envelops almost all associated laboratory data points, i.e. an upper bound approach. The conservative nature is moreover even emphasised in this approach, as the vertical axis presenting the CGR is typically logarithmic, i.e. a seemingly small rise of the CGR curve in the diagram leads to a considerable increase in the corresponding growth rate. All other available applicable CGR procedures for SCC in NPP components in BWR environment appear to be based on the same approach as the one used here, i.e. their temperature and environment dependent parameters have been defined so as to obtain an upper bound CGR curve, see procedures e.g. in refs. [32, 33]. Also, these CGR approaches mostly concern sensitised component materials, whereas presently in many/most NPP units in operation the primary circuit components have been replaced with ones of such materials that are not prone to become sensitised.

One possible way to relieve the conservatism in these CGR assessment procedures would be to apply best estimate approach, i.e. so that the CGR curves would rather be formed as to correspond to the mean values of the underlying laboratory data, than as the mentioned upper bound. This would require access to the underlying measurement data, however, which invariably are proprietary and not available, as CGR tests are expensive to perform, among other things because the test durations are typically of the scale of years. However, for the time being it seems that such best estimate approach, or optionally a probabilistic one, would be the best (and perhaps only) ways to relieve the conservatism in the mentioned CGR procedures. Hopefully this would be possible in the future, which obviously requires first gaining access to the mentioned CGR laboratory data sources. Having less conservative CGR procedures available would arguably lead to more realistic structural integrity and fitness-for-service analysis results. However, in these analysis procedures at least a reasonable level of conservative approach should be maintained at all times, so as to ensure a sufficient and adequate structural margin against e.g. weaker than designed materials, more severe than anticipated loads and longer than originally designed operational lifetimes.

### **Suggestions for further research**

In this study it is examined via numerical simulations how the WRSs alter over the years in plant operation in primary circuit component welds (e.g. to see if and how much they decrease), due to various typical/expected transient load cases. With such stress results, it is then examined what is their impact to the corresponding simulated CGRs. In the latter analyses a fracture mechanics based analysis tool is used.

Here an axisymmetric FEM model was used in the fully coupled thermal-stress/strain analyses. The next step could be to use a suitably optimised 3D FEM model in these analyses, or a coarser global 3D model in combination with a local but large enough and more densely meshed sub-model containing the region of interest, i.e. a weld.



One option to create local WRS distributions to a FEM model, that was due to work schedule limitations not attempted here, would be to use such values for the coefficient of thermal expansion in the weld region that the resulting stress field within the covered temperature range would match the desired WRS distribution. When using this approach the values of the coefficient of thermal expansion for the other material regions would be maintained in their original (i.e. correct) values or modified slightly.

Also the examined load history consisting of various anticipated load transients could be extended so as to cover more simulated years of simulated plant operation, and on the other hand a larger variety of different load transients, than in this study.

A primary circuit component weld of other type than considered here could be examined next, e.g. a nozzle/safe-end joint weld. There in addition to differing base material types on each side of the weld, also the inner cladding from the nozzle side would need to be taken into account.

One way to examine how the relatively high as-welded state WRSs alter over the years in plant operation in primary circuit component welds would be to carry out a literature study on the subject. This will be realised in the next phase of this project.

On the behalf of fracture mechanics based CGR analyses concerning IGSCC, the parameters  $C$  and  $n$ , which characterise the material properties as a function of temperature and environment in the used rate equations, could be reassessed applying best estimate and/or probabilistic approach. This would require, however, access to the underlying measurement data, which invariably are proprietary and not available. Hopefully these data will be made available in the future, at least partly.

Finally the formation of the WRSs themselves could be examined via numerical simulations. Relevant guidance concerning this task will be provided e.g. in the next edition/revision of the R6 Method, see R5/R6 Newsletter [35]. It is also planned that VTT participates with the resources of this project to the NRC Weld Residual Stress FEA Model Validation Program project [34], the WRS FEA simulation phase of which is planned to start this year.

## References

1. Cronvall, O. Review and Comparison of Welding Residual Stress Definitions, VTT Research report VTT-R-01415-08. Espoo, Finland, 2008. 102 p.
2. Section XI Task Group for Piping Flaw Evaluation, ASME Code. Evaluation of Flaws in Austenitic Steel Piping. Journal of Pressure Vessel Technology, Vol. 108, 1986. Pp. 352-366.
3. Shack, W., J. et al. Environmentally Assisted Cracking in Light Water Reactors: Annual Report, October 1981 – September 1982. NUREG/CR-3292, Washington D.C., U.S. Nuclear Regulatory Commission, June 1983.
4. British Standard BS 7910: 1999, Guide on methods for assessing the acceptability of flaws in fusion welded structures, 4th draft after public comment. England, 8 April, 1999.
5. R6 Method; Assessment of the Integrity of Structures containing Defects, Revision 4. 2004 update of 2001 edition. British Energy (BE).
6. Andersson, P. et al. 1998. A Procedure for Safety Assessment of Components with Cracks – Handbook, 3rd revised edition. SAQ/FoU-Report 96/08, SAQ Kontroll AB. Stockholm, Sweden. 104 p.
7. SINTAP; Structural Integrity Assessment Procedures for European Industry; Final Procedure: November 1999. Project funded by the European Union (EU) under the Brite-Euram Programme: Project No. BE95-1426, Contract No. BRPR-CT95-0024.
8. Barthelemy, J., Y., Janosch, J., J. Structural Integrity Assessment Procedures for European Industry; SINTAP; Task 4; Compendium of Residual Stress Profiles; Final Report: 18.5.1999. Project funded by the European Union (EU) under the Brite-Euram Programme: Project No. BE95-1426, Contract No. BRPR-CT95-0024. 40+18 pages.
9. American Petroleum Institute (API). Recommended practice for fitness-for-service. API 579. Washington, DC, American Petroleum Institute, 2000.
10. FITNET Fitness-for-Service PROCEDURE – FINAL DRAFT MK7. Editor(s) Koçak, M. et al. European Fitness-for-Service Thematic Network – FITNET. Germany. 1.5.2006.
11. Abaqus/Standard User's manual, Version 8.2. Dassault Systèmes Simulia Corp., 2008. Providence, Rhode Island, U.S.A.
12. Abaqus Theory manual, Version 8.2. Dassault Systèmes Simulia Corp., 2008. Providence, Rhode Island, U.S.A.
13. Cronvall, O. On welding residual stresses and their practical inclusion in structural integrity analyses. 20th International Conference on Structural Mechanics in Reactor Technology (SMiRT 20), Espoo, Finland, August 9-14, 2009, Paper 1798. 9 p. (To be published)
14. ASME Boiler and Pressure Vessel Code, Section II. 2005 Update of 2004 Edition.
15. Sattari-Far, I., Andersson, M. Cladding Effects on Structural Integrity of Nuclear Components. SKI Report 2006:23, Statens kärnkraftinspektion (SKI), 2006. 73 p.
16. Danko, J. C. 1990. A Review of Weld Residual Stresses in Austenitic Stainless Steel Pipes. Recent Trends in Welding Science and Technology. Proceedings of 2nd International Conference, Gatlinburg, TN, 14-18 May 1989. Pp. 113-118.



17. Lopez Martinez, L., Lin, R., Wang, D. & Blom, A. F. 1997. Investigation of Residual Stresses in As-Welded and TIG-Dressed Specimens Subjected to Static/Spectrum Loading. Welded High-Strength Steel Structures, Proceedings, First North European Engineering and Science Conference (NESCO 1). Stockholm, Sweden, 8-9 October 1997. Pp. 377-390.
18. Bradford, R. Through-thickness distributions of welding residual stresses in austenitic steel cylindrical butt welds. Proceedings of sixth international conference on residual stresses (ICRS-6). London: IOM Communications Ltd: 2000, p. 1373–381.
19. Bouchard, P., Bradford, R. Validated axial residual stress profiles for fracture assessment of austenitic stainless steel pipe girth welds, pressure vessel and piping. Proceedings of ASME conference, New York : ASME;2001;PVP-423: 93–99.
20. Dong, P., Brust, F. Welding residual stresses and effects on fracture in pressure vessel and piping components: a millennium review and beyond, ASME Trans. J. of Press. Vessel Technol. 2000; 122(3): 328–38.
21. Dong, P., Rahman, S., Wilkowski, G., Brickstad, B., Bergman, M., Bouchard, P., Chivers, T. Effect of weld residual stresses on crack opening area analysis of pipes for LBB applications. Proceedings of ASME pressure vessel and piping conference. New York: ASME; 1996; PVP-324. pp. 47–64.
22. Brickstad, B. The Use of Risk Based Methods for Establishing ISI-Priorities for Piping Components at Oskarshamn 1 Nuclear Power Station. SAQ/FoU-Report 99/05, SAQ Kontroll AB, 1999. 83 p.
23. Jansson, C., Morin, U. Assessment of Crack Growth Rates in Austenitic Stainless Steels in Operating BWRs. Proc. of Eighth International Symposium on Environmental Degradation of Materials in Nuclear Power Systems - Water Reactors. August 10 - 14, 1997. Amelia Island, Florida. Pp. 667-674.
24. ASME Boiler and Pressure Vessel Code Section III, Division 1, Article G-2000. 2005 Update of 2004 Edition.
25. European Commission. Nuclear Safety and Environment. Safe Management of NPP Ageing in the European Union, Final Report, 2001. 363 p.
26. Jones, H., R. (Editor). Stress-Corrosion Cracking. ASM International, Ohio, 1992. 448 p.
27. Congleton, J., Craig, I., H. "Corrosion Fatigue" in Corrosion Processes, Parkins, R., N., Ed., Applied Science Publishers, 1982.
28. Varfolomeyev, I. et al. BESIF 1.0: Stress Intensity Factors for Surface Cracks under 2D Stress Gradients. IWM-Report T 14/96, Fraunhofer-Institut für Werkstoffmechanik (IWM), July 1996. 42 p.
29. Busch, M. et al. KI-Factors and Polynomial Influence Functions for Axial and Circumferential Surface Cracks in Cylinders. IWM-Report T 18/94, Fraunhofer-Institut für Werkstoffmechanik (IWM), October 1994. 41 p.
30. Busch, M. et al. Polynomial Influence Functions for Surface Cracks in Pressure Vessel Components. IWM-Report Z 11/95, Fraunhofer-Institut für Werkstoffmechanik (IWM), January 1995. 88 p.
31. Vepsä, A. Verification of the stress intensity factors calculated with the VTTBESIT software. Technical Research Centre of Finland (VTT), Research Group Structural Integrity, Research Report TUO72-044578. 40+2 p.

32. Morin, U., Jansson, C., Bengtsson, B. Crack Growth Rates for Ni-base Alloys with the Application to an Operating BWR. Sixth International Symposium on Environmental Degradation of Materials in Nuclear Power Systems - Water Reactor Systems. August 1 - 5, 1993. San Diego, California. Pp. 373-378.
33. Japanese Society of Mechanical Engineers, JSME Codes for Nuclear Power Generation Facilities, JSME S NAI-2004, Rules of Fitness-for-Service for Nuclear Power Plants. 2004, JSME, Tokyo, Japan.
34. Csontos, A. NRC Weld Residual Stress FEA Model Validation Program. Office of Nuclear Regulatory Research, U.S. Nuclear Regulatory Commission. Meeting presentation concerning project update, U.S.A., July 30, 2008. 17 p.
35. R5 and R6 Panels. R5/R6 Newsletter. Number 38, January 2009. 11 p.